

Oscillating-charged Andreev Bound States and Their Appearance in UTe_2

Satoshi Ando,^{1,*} Shingo Kobayashi,^{2,*} Andreas P. Schnyder,³ Yasuhiro Asano,⁴ and Satoshi Ikegaya^{1,5,*}

¹*Department of Applied Physics, Nagoya University, Nagoya 464-8603, Japan*

²*RIKEN Center for Emergent Matter Science, Wako, Saitama, 351-0198, Japan*

³*Max-Planck-Institut für Festkörperforschung, Heisenbergstrasse 1, D-70569 Stuttgart, Germany*

⁴*Department of Applied Physics, Hokkaido University, Sapporo 060-8628, Japan*

⁵*Institute for Advanced Research, Nagoya University, Nagoya 464-8601, Japan*

(Dated: March 5, 2024)

In a superconductor with a sublattice degree of freedom, we find unconventional Andreev bound states whose charge density oscillates in sign between the two sublattices. The appearance of these oscillating-charged Andreev bound states is characterized by a Zak phase, rather than a conventional topological invariant. In contrast to conventional Andreev bound states, for oscillating-charged Andreev bound states the proportionality between the electron-like spectral function, the local density of states and the tunneling conductance is broken. We examine the possible appearance of these novel Andreev bound states in UTe_2 and locally noncentrosymmetric superconductors.

Introduction.—The characterization of electronic states in terms of topology has been a hot research topic [1–6] in condensed matter physics. By the bulk-boundary correspondence, a nontrivial topological number in the bulk implies the appearance of gapless states at the surface. One example is the three-dimensional winding number that describes the topology and surface states of the B phase of superfluid ^3He [7, 8]. Another example is the Zak phase (or Berry phase) [9, 10] which describes the quantum mechanical properties of the electronic states in insulators and (semi-)metals. For instance, a quantized Zak phase of π indicates the topological nontriviality of one dimensional inversion symmetric insulators [10]. In the absence of inversion and mirror symmetry, however, the Zak phase is not quantized. Nevertheless it is a measurable quantity as it is related to the bulk polarization, as described by the modern theory of polarization [11–16]. At the surface, the Zak phase leads to in-gap surface states and charge accumulation, whereby the surface charge is defined only up to an integer multiple of 2π [12, 17–19] (see also Refs. [20, 21] for alternative characterizations of surface topology).

So far, the Zak phase has been mostly used in insulators and semimetals to describe their polarization and topological properties. The Zak phase can also be used to characterize superconductors [4], whose particle-hole symmetry quantizes it to zero or π . However, unquantized Zak phases have, to the best of our knowledge, not been discussed in the context of superconductors.

In this Letter, we show that the topology of superconductors with a sublattice degree of freedom can be characterized by an *unquantized* Zak phase, which by the bulk-boundary correspondence leads to a novel type of Andreev bound states (ABSs) at the surface. Such systems are described by Bogoliubov-de Gennes (BdG) Hamiltonians that can be separated into two subsectors. While particle-hole symmetry is satisfied for the full Hamiltonian, each subsector breaks it, thereby al-

lowing the definition of a *unquantized* Zak phase for each subsector. By the bulk-boundary correspondence this unquantized Zak phase leads to unusual surface ABS whose key properties are: (i) The ABS energy is in general non-zero, (ii) the charge density of the ABSs oscillates in sign between the two sublattices [see Figs. 1(a)–(c)], and (iii) the proportionality between the electron-like charge density ρ_e , the local density of states ρ , and the tunneling conductance G is broken [see Figs. 1(d)–(f)]. Due to the first two properties we call these ABS oscillating-charged Andreev bound states (OCABS). The third property is particularly remarkable, since the proportionality between ρ_e , ρ , and G has been up to now accepted as a general feature of superconductors, as described by quasiclassical theory [22–24]. Finally we discuss the possible appearance of the OCABS in the superconductor UTe_2 [25], which has attracted much attention recently due to a field-induced reentrant spin-triplet superconductivity [26–32].

Minimal model.—First, we introduce a generic model with sublattice degree of freedom that exhibits OCABS with unquantized Zak phase. We use the Rice-Mele model as the starting point [41], since it is the minimal model of an insulator harboring in-gap states characterized by the Zak phase. Our basic scheme is to replace the inter-sublattice hopping terms in the Rice-Mele Hamiltonian with the inter-sublattice pair potential. Specifically, we consider a sublattice superconductor illustrated in Fig. 1(a). There are two sites within the primitive unit cells, i.e., the a - and b -sites located at x and $x + \frac{1}{2}a_0$, respectively, forming two distinct sublattices. In what follows, we set the lattice constant a_0 to one, such that x takes on integer values. For simplicity we consider first the extreme case, where finite hopping only occurs between sites of the same sublattice [single lines in Fig. 1(a)], while pairing happens only between different sublattices [double lines in Fig. 1(a)]. This extreme limit may be unrealistic, but it is useful to bring out the key properties of the OCABSs. A straightforward ex-

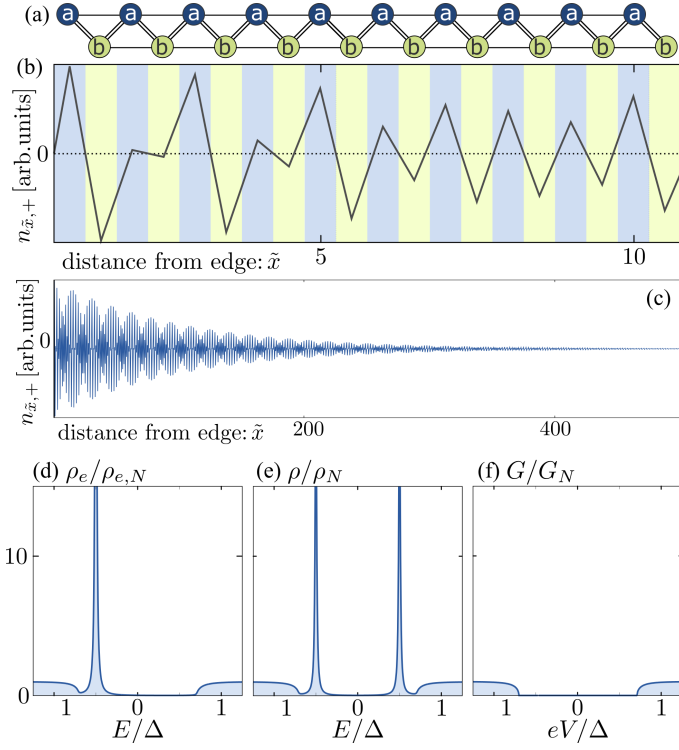


FIG. 1. (a) Schematic image of the sublattice superconductor. The single (double) line describes the coupling through t (Δ). (b) and (c) Charge density of OCABS, i.e., $n_{\tilde{x},+}$ defined by Eq. (7), as a function of the distance from the edge. We choose $\mu = 0.1t$ and $\Delta = 0.01t$. In (b) and (c), the results for $1 \leq \tilde{x} \leq 10 + \frac{1}{2}$ and that for $1 \leq \tilde{x} \leq 500 + \frac{1}{2}$ are plotted, respectively. (d) $\rho_e/\rho_{e,N}$ and (e) ρ/ρ_N as a function of the energy. (f) G/G_N as a function of the bias voltage.

tension of our minimal model describes a locally noncentrosymmetric superconductor [33–35] with an inter-layer pairing [36, 37], which is proposed to describe the superconductor CeRh_2As_2 [38, 39]. In the Supplemental Material (SM) [40], we show the explicit BdG Hamiltonian for the locally noncentrosymmetric superconductor and demonstrate the appearance of the OCABSs. Furthermore, we will show later that the low-energy excitations of superconducting UTe_2 [25] are effectively described by our minimal model. Let us consider the BdG Hamiltonian of our minimal model in momentum space:

$$H = \frac{1}{2} \sum_k [\Psi_{k,+}^\dagger, \Psi_{k,-}^\dagger] \begin{bmatrix} h_{k,+} & 0 \\ 0 & h_{k,-} \end{bmatrix} \begin{bmatrix} \Psi_{k,+} \\ \Psi_{k,-} \end{bmatrix},$$

$$h_{k,s} = \begin{bmatrix} t \cos(k) - \mu & \Delta e^{-is\frac{k}{2}} \cos(k/2) \\ \Delta e^{is\frac{k}{2}} \cos(k/2) & -t \cos(k) + \mu \end{bmatrix}, \quad (1)$$

$$\Psi_{k,+} = [\psi_{k,a}, \psi_{-k,b}^\dagger]^T, \quad \Psi_{k,-} = [\psi_{k,b}, \psi_{-k,a}^\dagger]^T$$

where $s = +1$ (-1), $\psi_{k,\alpha}$ is the annihilation operator of an electron at sublattice α with momentum k , t denotes the hopping integral, μ represents the chemical potential,

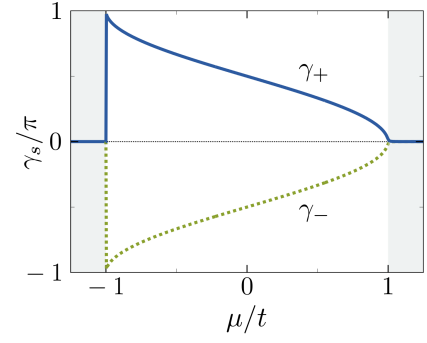


FIG. 2. Zak phase as a function of the chemical potential.

and Δ is the pair potential. We remark that the block component $h_{k,s}$ has a form similar to the Hamiltonian of the Rice-Mele model [41], where the inter-sublattice hopping terms and the on-site potentials are replaced by the inter-sublattice pair potential and the normal-state kinetic term, respectively. The particle-hole symmetry operator in this basis is given by

$$\tilde{C} = \begin{bmatrix} 0 & C \\ C & 0 \end{bmatrix}, \quad C = \begin{bmatrix} 0 & 1 \\ -1 & 0 \end{bmatrix} \mathcal{K}, \quad (2)$$

where \mathcal{K} represents the complex conjugation operator and $\tilde{C}^2 = -1$, due to the absence of spin-degrees of freedom. Importantly, the particle-hole symmetry is broken within each block component, $Ch_{k,s}C^{-1} = -h_{-k,-s} \neq -h_{k,s}$, while the operation of \tilde{C} additionally interchanges the two blocks. Thus, the Zak phase defined for each block,

$$\gamma_s = i \int_{-\pi}^{\pi} dk \langle u_{k,s} | \partial_k | u_{k,s} \rangle, \quad (3)$$

is not quantized and can take on any value between $-\pi$ and π . Here $|u_{k,s}\rangle$ describes the occupied eigenstate of $h_{k,s}$ and satisfies the periodic boundary condition $|u_{k,s}\rangle = |u_{k+2\pi,s}\rangle^*$. In Fig. 2, we show γ_s as a function of μ , where $\Delta = 0.001t$. We indeed obtain $\gamma_s \neq 0, \pi$ for $|\mu| < t$, whereas $\gamma_s = 0$ for $|\mu| > t$, due to the absence of Fermi points. Here, particle-hole symmetry imposes $\gamma_+ + \gamma_- = 0 \pmod{2\pi}$ since the full Hamiltonian is topologically trivial. The fractional part of γ_s , i.e., $\gamma_s/2\pi \pmod{1}$, characterizes the increase of the probability density at the surface [17–19]. The BdG Hamiltonian in Eq. (24) has the complete block-diagonal form. Even in the presence of small block-off diagonal components, we can still define the unquantized Zak phase in terms of a projection, i.e., a projection into the block diagonal

* In this paper, we only focus on the intercellular part of the Zak phase [17].

space, before computing the Zak phase, as is the case with the spin Chern number [42–44].

To see the relation between γ_s and ABSs, we solve the BdG equation in real space:

$$T_s \varphi_{x-1,s} + T_s^\dagger \varphi_{x+1,s} + K \varphi_{x,s} = E_s \varphi_{x,s}, \quad (4)$$

with

$$T_s = \begin{bmatrix} \frac{t}{2} & \frac{(1+s)\Delta}{4} \\ \frac{(1-s)\Delta}{4} & -\frac{t}{2} \end{bmatrix}, \quad K = \begin{bmatrix} -\mu & \frac{\Delta}{2} \\ \frac{\Delta}{2} & \mu \end{bmatrix}, \quad (5)$$

$$\varphi_{x,+} = [u_{x,+}, v_{x+\frac{1}{2},+}]^T, \quad \varphi_{x,-} = [u_{x+\frac{1}{2},-}, v_{x,-}]^T,$$

$$u_{x+\frac{1}{2},+} = v_{x,+} = u_{x,-} = v_{x+\frac{1}{2},-} = 0,$$

where $u_{x,s}$ ($v_{x,s}$) denotes the electron (hole) component in the sublattice a , and $u_{x+\frac{1}{2},s}$ ($v_{x+\frac{1}{2},s}$) represents the electron (hole) component in the sublattice b . We consider the semi-infinite system for $x > 0$ and apply an open-boundary condition, $\varphi_{0,s} = 0$. We indeed find the solutions of the ABSs for $|\mu| < t$, where the energy eigenvalue and eigenvector are given by

$$E_s = -s \frac{\Delta}{2t} (t + \mu), \quad \varphi_{x,s} = \begin{bmatrix} 1 \\ -s \end{bmatrix} \phi_x, \quad (6)$$

respectively. The derivation of ABSs and the explicit form of the real function ϕ_x are relegated to the SM [40]. Here we focus on the charge density of the ABSs defined by

$$n_{\tilde{x},s} = e(|u_{\tilde{x},s}|^2 - |v_{\tilde{x},s}|^2), \quad (7)$$

with $\tilde{x} = x$ or $x + \frac{1}{2}$. The ABSs of $\varphi_{x,+(-)}$ contains the electron component only at the a -sublattices (b -sublattices) and hole component only at the b -sublattices (a -sublattices). As a result, we obtain

$$n_{x,s} = es|\phi_x|^2, \quad (8)$$

$$n_{x+\frac{1}{2},s} = -es|\phi_x|^2.$$

Remarkably, as also shown in Fig. 1(b), the charge density of the ABSs changes sign for each sublattice. This establishes the oscillating-charge nature of the OCABS. The OCABS is distinguished from the surface charge density of the original Rice-Mele model, which only has the electron components at the a - and b -sublattices.

To examine further properties of the OCABSs, we study three quantities: the electron part of the spectral function ρ_e , the local density of states ρ , and the tunneling conductance G . The proportionality among these three quantities has been proven within a quasi-classical theory of superconductivity [22–24] and has been accepted as a generic feature of superconductivity. However, we will show that the OCABSs break this proportionality completely. We first examine ρ_e and ρ , respec-

tively, given by

$$\rho_e(\tilde{x}, E) = -\frac{1}{\pi} \text{Im}[g(\tilde{x}, \tilde{x}, E)], \quad (9)$$

$$\rho(\tilde{x}, E) = -\frac{1}{\pi} \text{Im}[g(\tilde{x}, \tilde{x}, E) + \underline{g}(\tilde{x}, \tilde{x}, E)], \quad (10)$$

where

$$\mathcal{G}(\tilde{x}, \tilde{x}', E) = \begin{bmatrix} g(\tilde{x}, \tilde{x}', E) & f(\tilde{x}, \tilde{x}', E) \\ \underline{f}(\tilde{x}, \tilde{x}', E) & \underline{g}(\tilde{x}, \tilde{x}', E) \end{bmatrix}, \quad (11)$$

represents the retarded Gorkov Green's function. By focusing on $E \approx E_s$ and extracting the contributions from the OCABSs to the Green's function, we approximately obtain

$$g(x, x, E) = \underline{g}(x + \frac{1}{2}, x + \frac{1}{2}, E) = \frac{|\phi_x|^2}{E + E_c + i\delta}, \quad (12)$$

$$g(x + \frac{1}{2}, x + \frac{1}{2}, E) = \underline{g}(x, x, E) = \frac{|\phi_x|^2}{E - E_c + i\delta},$$

where $E_c = |E_s|$. The detailed derivation of Eq. (12) is discussed in the SM [40]. At the outermost site belonging to the a -sublattice (i.e., $x = 1$), the wave function of the OCABS with negative (positive) energy have only electron (hole) components. Accordingly, $g(1, 1, E)$ has a pole only at negative energy (i.e., $E = -E_c$), while $\underline{g}(1, 1, E)$ has a pole only at positive energy (i.e., $E = E_c$). In Fig. 1(d) and Fig. 1(e), we show $\rho_e(x, E)$ and $\rho(x, E)$ at the outermost site (i.e., $x = 1$) as a function of energy, where we choose $\mu = 0$ and $\Delta = 0.001$. The Green's functions are computed numerically by using recursive Green's function techniques [45, 46]. The results are normalized by the value calculated with $\Delta = E = 0$. The electron part of the spectral function $\rho_e(1, E)$ has the asymmetric spectrum [47–49], where the peak exists only at $E = -E_c$. In contrast, the local density of states $\rho(1, E)$ has symmetric peaks at $E = \pm E_c$. We also remark that ρ_e at the second-outermost site (i.e., $x = 1 + \frac{1}{2}$) exhibits the peak only at $E = +E_c$, which manifests the oscillating-charge nature of the OCABSs. Next, we discuss the tunneling conductance G . We consider a normal-metal lead attached to the outermost site of the superconductor (i.e., the a -sublattice at $x = 1$). We describe the normal-metal lead by $H_N = -t \sum_x (a_{x+1}^\dagger a_x + \text{h.c.})$, where a_x denotes the annihilation operator of an electron in the normal-metal with x being integer numbers for $x < 0$. The coupling between the lead and superconductor is described by $H_T = -t' (\psi_{\tilde{x}=1}^\dagger a_{x=0} + \text{h.c.})$, where $\psi_{\tilde{x}}$ denotes the annihilation operator of an electron at \tilde{x} in the superconductor. We calculate G using the Blonder–Tinkham–Klapwijk formula [50],

$$G = \frac{e^2}{h} [1 - |b(E)|^2 + |a(E)|^2]_{E=eV}, \quad (13)$$

where $a(E)$ and $b(E)$ represent the Andreev and normal reflection coefficients at energy E . These scattering coefficients are computed numerically using recursive

Green's function techniques [45, 46]. We assume the low-transparency interface with $t' = 0.02t$. The results are normalized by the normal conductance calculated by setting $\Delta = eV = 0$. In Fig. 1(f), we show the tunneling conductance G as a function of the bias voltage. Remarkably, G does not exhibit any peaks for $|eV| < \Delta$. To understand the result, we consider a generic form of the tunneling conductance in the presence of the ABS: when an ABS exists at $E = E_B$, the tunneling conductance at $eV \approx E_B$ is represented by [51, 52]

$$G \approx \frac{e^2}{h} \frac{8(|U||V|)^2}{(eV - E_B)^2 + (|U|^2 + |V|^2)^2}, \quad (14)$$

where the detailed derivation of Eq. (14) is also discussed in the SM [40]. The parameter U (V) characterizes the couplings between the incident electron and the electron (hole) component of the ABS. The tunneling conductance is finite only when both U and V are finite (i.e., $|U||V| \neq 0$). For the OCABS, however, the electron and hole components do not exist at the same site owing to its oscillating-charge nature. Thus, we obtain $G = 0$ owing to $|U||V| = 0$ (see the SM for a detailed discussion). Eventually, we demonstrate that in the presence of the OCABSs, ρ_e , ρ , and G exhibit clearly different spectra.

Superconductor UTe_2 .—Next, we discuss the possible appearance of OCABSs in the superconductor UTe_2 . We consider the BdG Hamiltonian proposed in Ref. [25]:

$$\begin{aligned} H &= \frac{1}{2} \sum_{\mathbf{k}, \sigma} [\psi_{\mathbf{k}\sigma}^\dagger, \psi_{-\mathbf{k}\bar{\sigma}}^\dagger] H_{\mathbf{k}} \begin{bmatrix} \psi_{\mathbf{k}\sigma} \\ \psi_{-\mathbf{k}\bar{\sigma}}^* \end{bmatrix}, \\ \psi_{\mathbf{k}\sigma}^\dagger &= [\psi_{\mathbf{k},\sigma,a,1}^\dagger, \psi_{\mathbf{k},\sigma,a,2}^\dagger, \psi_{\mathbf{k},\sigma,b,1}^\dagger, \psi_{\mathbf{k},\sigma,b,2}^\dagger], \\ H_{\mathbf{k}} &= \begin{bmatrix} \tilde{h}_{\mathbf{k}} & \tilde{h}_{\Delta} \\ \tilde{h}_{\Delta}^\dagger & -\tilde{h}_{-\mathbf{k}}^* \end{bmatrix}, \end{aligned} \quad (15)$$

with

$$\begin{aligned} \tilde{h}_{\mathbf{k}} &= \begin{bmatrix} \hat{K}_{\mathbf{k}} & \hat{T}_{\mathbf{k}}^\dagger \\ \hat{T}_{\mathbf{k}} & \hat{K}_{\mathbf{k}} \end{bmatrix}, \quad \hat{K}_{\mathbf{k}} = \begin{bmatrix} \epsilon_{\mathbf{k}} & m_g \\ m_g & \epsilon_{\mathbf{k}} \end{bmatrix}, \\ \hat{T}_{\mathbf{k}} &= e^{i\frac{k_x}{2}} e^{i\frac{k_y}{2}} e^{i\frac{k_z}{2}} \begin{bmatrix} 0 & f_{g,\mathbf{k}} - if_{z,\mathbf{k}} \\ f_{g,\mathbf{k}} + if_{z,\mathbf{k}} & 0 \end{bmatrix}, \end{aligned} \quad (16)$$

$$\begin{aligned} \epsilon_{\mathbf{k}} &= t_1 \cos(k_x) + t_2 \cos(k_y) - \mu, \\ f_{g,\mathbf{k}} &= t_3 \cos(k_x/2) \cos(k_y/2) \cos(k_z/2), \\ f_{z,\mathbf{k}} &= t_z \cos(k_x/2) \cos(k_y/2) \sin(k_z/2), \end{aligned}$$

and

$$\tilde{h}_{\Delta} = \begin{bmatrix} \hat{\Delta} & 0 \\ 0 & \hat{\Delta} \end{bmatrix}, \quad \hat{\Delta} = \begin{bmatrix} 0 & \Delta \\ -\Delta & 0 \end{bmatrix}, \quad (17)$$

where $\psi_{\mathbf{k},\sigma,\alpha,l}$ is the annihilation operator of an electron with momentum \mathbf{k} with spin σ at the l -th rung of the sublattice α . The index $\bar{\sigma}$ means the opposite spin of σ . The rung degree of freedom is originated from the two inequivalent U sites that constitute the ladder rung [25].

Note that Eq. (96) is modified to take into account the sublattice degrees of freedom explicitly. The parameters are chosen as $(\mu, t_1, t_2, m_0, t_3, t_z) = (-0.129, -0.0892, 0.0678, -0.062, 0.0742, -0.0742)$ [25]. We assume the inter-rung-odd spin-triplet s -wave pair potential belonging to A_u of the D_{2h} point-group symmetry, where we choose $\Delta = 0.001$. As shown in the SM [40], qualitatively equivalent results are also obtained for the B_{2u} and B_{3u} pairings. Here we ignore the insignificant spin-orbit coupling terms [25], where the appearance of the OCABSs in the presence of the spin-orbit coupling potentials is demonstrated in the SM [40].

Although the Hamiltonian $H_{\mathbf{k}}$ has the form of a complex 8×8 matrix, the energy bands are two-fold degenerate at the Brillouin zone boundary, i.e., $k_z = \pi$ due to the sublattice structure. Thus, we can analytically construct a low-energy effective Hamiltonian at $k_z = \pi$, which displays the equivalence between the model of UTe_2 in Eq. (96) and our minimal model in Eq. (24). To this end, by applying a unitary transformation (see the SM [40]), $H_{\mathbf{k}}$ at $k_z = \pi$ is deformed into a band basis:

$$\begin{aligned} H_{\mathbf{q}}^{\text{band}} &= \begin{bmatrix} \check{H}_{\mathbf{q},+} & 0 \\ 0 & \check{H}_{\mathbf{q},-} \end{bmatrix} \\ \check{H}_{\mathbf{q},s} &= \begin{bmatrix} \epsilon_{\mathbf{q}} + sV_{\mathbf{q}} & 0 & s\Delta\alpha_{\mathbf{q},-} & -s\Delta\beta_{\mathbf{q}} \\ 0 & \epsilon_{\mathbf{q}} - sV_{\mathbf{q}} & s\Delta\beta_{\mathbf{q}} & s\Delta\alpha_{\mathbf{q},+} \\ s\Delta\alpha_{\mathbf{q},+} & s\Delta\beta_{\mathbf{q}} & -\epsilon_{\mathbf{q}} - sV_{\mathbf{q}} & 0 \\ -s\Delta\beta_{\mathbf{q}} & s\Delta\alpha_{\mathbf{q},-} & 0 & -\epsilon_{\mathbf{q}} + sV_{\mathbf{q}} \end{bmatrix}, \\ V_{\mathbf{q}} &= \sqrt{m_g^2 + f_{z,\mathbf{q}}^2}, \\ \alpha_{\mathbf{q},\pm} &= e^{\pm ik_x/2} e^{\pm ik_y/2} \frac{f_{z,\mathbf{q}}}{V_{\mathbf{q}}}, \quad \beta_{\mathbf{q}} = \frac{m_g}{V_{\mathbf{q}}}, \end{aligned} \quad (18)$$

where $\mathbf{q} = (k_x, k_y, k_z = \pi)$. With the present parameter choice, the normal-state of $\epsilon_{\mathbf{q}} + V_{\mathbf{q}}$ pinches off from the Fermi level, i.e., $\epsilon_{\mathbf{q}} + V_{\mathbf{q}} > 0$ irrespective of \mathbf{q} . Thus, the low-energy excitation is effectively described by the 2×2 Hamiltonian,

$$\hat{h}_{\mathbf{q},s}^{\text{eff}} = \begin{bmatrix} \epsilon_{\mathbf{q}} - V_{\mathbf{q}} & -s\Delta\alpha_{\mathbf{q},-s} \\ -s\Delta\alpha_{\mathbf{q},-s}^* & -\epsilon_{\mathbf{q}} + V_{\mathbf{q}} \end{bmatrix}. \quad (19)$$

Interestingly, although we start from the momentum-independent pair potential, the resultant superconducting gap in the band basis ends up with the momentum-dependent inter-sublattice pair potential:

$$s\Delta\alpha_{\mathbf{q},-s} \propto e^{-si\frac{k_x}{2}} e^{-si\frac{k_y}{2}} \cos(k_x/2) \cos(k_y/2), \quad (20)$$

where the inter-sublattice pair potential is attributed to the inter-rung pairing and the inter-sublattice inter-rung hopping terms. For a fixed $k_{x(y)}$, the effective Hamiltonian in Eq. (19) is equivalent to Eq. (24). Therefore, we expect the appearance of the OCABSs associated with the Zak phase.

To verify this expectation, we calculate the Zak phase

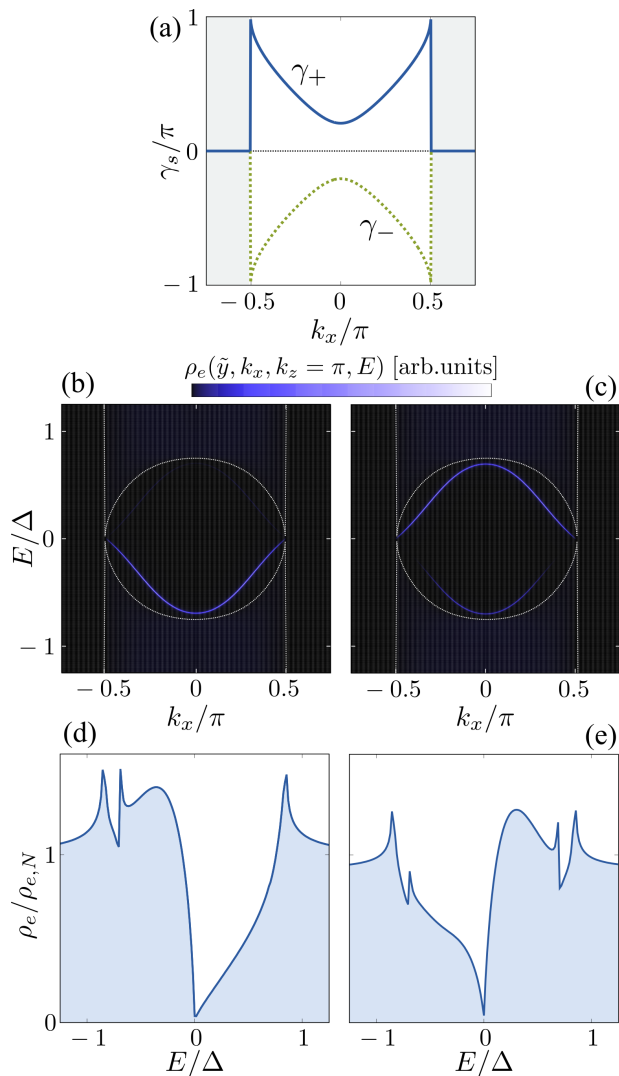


FIG. 3. (a) Zak phase as function of k_x . (b)-(c) Electron part of angle-resolved spectral function at $k_z = \pi$ as a function of k_x and the energy E . (d)-(e) Electron part of spectral function as a function of the energy E , where the contributions from different k_x and k_z are integrated. In (b) and (d), we show the results for the outermost site, i.e., $\tilde{y} = 1$, and in (c) and (e), we plot the results for the second-outermost site $\tilde{y} = 1 + \frac{1}{2}$.

for the effective Hamiltonian,

$$\gamma_{s,k_x} = i \int_{-\pi}^{\pi} dk_y \langle u_{\mathbf{q},s} | \partial_{k_y} | u_{\mathbf{q},s} \rangle, \quad (21)$$

which characterizes the probability density accumulation at the surface parallel to the x direction, where $|u_{\mathbf{q},s}\rangle$ describes the occupied state of $\tilde{h}_{\mathbf{q},s}^{\text{eff}}$. As shown in Fig. 3(a), the Zak phase becomes finite for $|k_x| < 0.5\pi$. In Fig. 3(b) and 3(c), we show the electron part of angle-resolved spectral function $\rho_e(\tilde{y}, k_x, k_z = \pi, E)$ as a function of k_x and energy E , where $\tilde{y} = y$ or $y + \frac{1}{2}$ measures the distant from the surface with y being an integer number. The Green's function is calculated using the recursive Green's

function techniques [45, 46]. In Fig. 3(b) and 3(c), the result for the outermost site $\rho_e(1, k_x, \pi, E)$ and that for the second-outermost site $\rho_e(1 + \frac{1}{2}, k_x, \pi, E)$ are plotted, respectively. The dotted white lines denote the bulk dispersion, obtained by diagonalizing $H_{\mathbf{q}}$ in Eq. (18). We find the ABSs for $|k_x| < 0.5\pi$ where the Zak phase is finite. Moreover, $\rho_e(\tilde{y}, k_x, \pi, E)$ for the outermost (second-outermost) site has the significant enhancement only for $E < 0$ ($E > 0$), which means that the resultant ABSs exhibit the oscillating-charge nature. In Figs. 3(d) and 3(e), we show the electron part of the spectral function at $\tilde{y} = 1$ and $\tilde{y} = 1 + \frac{1}{2}$ as a function of E , respectively. The contributions from different k_x and k_z are integrated, i.e., $\rho_e(\tilde{y}, E) = \sum_{k_x, k_z} \rho_e(\tilde{y}, k_x, k_z, E)$. For $\rho_e(\tilde{y}, E)$ at the outermost (second-outermost) site, we find the significant hump only for $E < 0$ ($E > 0$). Although the low-energy effective Hamiltonian in Eq. (19) is valid only at $k_z = \pi$, we confirm that the signature of the OCABSs remains significant even when the contributions from various k_z are integrated.

Summary.—In summary, we have demonstrated the appearance of the unconventional ABSs characterized by the Zak phase, i.e., OCABSs. The OCABSs cause the clear breakdown in the proportionality among ρ_e , ρ , and G . We also describe the possible emergence of OCABSs in the explicit model of UTe_2 and locally non-centrosymmetric superconductors. Proposing conclusive experiments for observing the oscillating-charge nature of the OCABSs would be a desirable future task. Finding further material candidates hosting the OCABSs is also an important future work; superconducting ladder systems [53–60] and superconducting layered systems [61–68] are promising candidates. Our results indicate a new direction for developing the physics of ABSs beyond the predictions of topological numbers.

We thank Y. Tanaka and L. Katayama for the fruitful discussions. S.A. is supported by the Nagoya University Interdisciplinary Frontier Fellowship (Grant No.JPMJFS2120). S.I. is supported by the Grant-in-Aid for JSPS Fellows (JSPS KAKENHI Grant No. JP22KJ1507).

* These authors contributed equally to this work.

- [1] M. Z. Hasan and C. L. Kane, Rev. Mod. Phys. **82**, 3045 (2010).
- [2] X.-L. Qi and S.-C. Zhang, Rev. Mod. Phys. **83**, 1057 (2011).
- [3] Y. Tanaka, M. Sato, and N. Nagaosa, J. Phys. Soc. Jpn. **81**, 011013 (2012).
- [4] M. Sato and S. Fujimoto, J. Phys. Soc. Jpn. **85**, 072001 (2016).
- [5] C.-K. Chiu, J. C. Y. Teo, A. P. Schnyder, and S. Ryu, Rev. Mod. Phys. **88**, 035005 (2016).
- [6] M. Sato and Y. Ando, Rep. Prog. Phys. **80**, 076501 (2017).

- [7] G. E. Volovik, *The universe in a helium droplet* (Clarendon Press, 2003), ISBN 0199564841.
- [8] A. P. Schnyder, S. Ryu, A. Furusaki, and A. W. W. Ludwig, Phys. Rev. B **78**, 195125 (2008).
- [9] M. V. Berry, Proc. R. Soc. Lond. A **392**, 45 (1984).
- [10] J. Zak, Phys. Rev. Lett. **62**, 2747 (1989).
- [11] R. D. King-Smith and D. Vanderbilt, Phys. Rev. B **47**, 1651 (1993).
- [12] D. Vanderbilt and R. D. King-Smith, Phys. Rev. B **48**, 4442 (1993).
- [13] R. Resta, Rev. Mod. Phys. **66**, 899 (1994).
- [14] R. Resta and D. Vanderbilt, Theory of Polarization: A Modern Approach (Springer, New York, 2007), pp. 31–68.
- [15] G. Ortiz and R. M. Martin, Phys. Rev. B **49**, 14202 (1994).
- [16] D. Vanderbilt, Berry Phases in Electronic Structure Theory (Cambridge University Press, Cambridge, 2018).
- [17] J.-W. Rhim, J. Behrends, and J. H. Bardarson Phys. Rev. B **95**, 035421 (2017).
- [18] G. vanMiert and C. Ortix Phys. Rev. B **96**, 235130 (2017).
- [19] H. Watanabe and M. Oshikawa, Phys. Rev. X **8**, 021065 (2018).
- [20] J.-W. Rhim, J. H. Bardarson, and R.-J. Slager, Phys. Rev. B **97**, 115143 (2018).
- [21] M. Pletyukhov, D. M. Kennes, J. Klinovaja, D. Loss, and H. Schoeller, Phys. Rev. B **101**, 161106(R) (2020); *ibid.* **101**, 165304 (2020).
- [22] Y. Tanaka and S. Kashiwaya, Phys. Rev. Lett. **74**, 3451 (1995).
- [23] Y. Tanaka and S. Kashiwaya, Phys. Rev. B **53**, 9371 (1996).
- [24] S. Kashiwaya and Y. Tanaka, Rep. Prog. Phys. **63**, 1641 (2000).
- [25] T. Shishidou, H. G. Suh, P. M. R. Brydon, M. Weinert, and D. F. Agterberg, Phys. Rev. B **103**, 104504 (2021).
- [26] S. Ran, C. Eckberg, Q. -P. Ding, Y. Furukawa, T. Metz, S. R. Saha, I. -L. Liu, M. Zic, H. Kim, J. Paglione, N. P. Butch, Science **365**, 684–687 (2019).
- [27] T. Metz, S. Bae, S. Ran, I. -L. Liu, Y. S. Eo, W. T. Fuhrman, D. F. Agterberg, S. M. Anlage, N. P. Butch, and J. Paglione, Phys. Rev. B **100**, 220504 (2019).
- [28] S. Sundar, S. Gheidi, K. Akintola, A. M. Côté, S. R. Dunsiger, S. Ran, N. P. Butch, S. R. Saha, J. Paglione, and J. E. Sonier, Phys. Rev. B **100**, 140502(R) (2019).
- [29] D. Aoki, A. Nakamura, F. Honda, D. Li, Y. Homma, Y. Shimizu, Y. J. Sato, G. Knebel, J.-P. Brison, A. Pourret, D. Braithwaite, G. Lapertot, Q. Niu, M. Valiäka, H. Harima, and J. Flouquet, J. Phys. Soc. Jpn. **88**, 043702 (2019).
- [30] I. M. Hayes, D. S. Wei, T. Metz, J. Zhang, Y. S. Eo, S. Ran, S. R. Saha, J. Collini, N. P. Butch, D. F. Agterberg, A. Kapitulnik, J. Paglione, Science **373**, 797–801 (2021).
- [31] C. Duan, R. E. Baumbach, A. Podlesnyak, Y. Deng, C. Moir, A. J. Breindel, M. B. Maple, E. M. Nica, Q. Si, and P. Dai Nature **600**, 63–640 (2021).
- [32] D. Aoki, J.-P. Brison, J. Flouquet, K. Ishida, G. Knebel, Y. Tokunaga, and Y. Yanase, J. Phys.: Condens. Matter **34** 243002 (2022).
- [33] M. H. Fischer, F. Loder, and M. Sigrist, Phys. Rev. B **84**, 184533 (2011).
- [34] M. Sigrist, D. F. Agterberg, M. H. Fischer, J. Goryo, F. Loder, S.-H. Rhim, D. Maruyama, Y. Yanase, T. Yoshida, and S. J. Youn, J. Phys. Soc. Jpn. **83**, 061014 (2014).
- [35] M. H. Fischer, M. Sigrist, D. F. Agterberg, and Y. Yanase, Annu. Rev. Condens. Matter Phys. **14**, 153 (2023).
- [36] D. Möckli and A. Ramires, Phys. Rev. Research **3**, 023204 (2021).
- [37] D. Möckli and A. Ramires, Phys. Rev. B **104**, 134517 (2021).
- [38] S. Khim, J. F. Landaeta, J. Banda, N. Bannor, M. Brando, P. M. R. Brydon, D. Hafner, R. Küchler, R. Cardoso-Gil, U. Stockert, A. P. Mackenzie, D. F. Agterberg, C. Geibel, and E. Hassinger, Science **373**, 1012 (2021).
- [39] J. F. Landaeta, P. Khanenko, D. C. Cavanagh, C. Geibel, S. Khim, S. Mishra, I. Sheikin, P. M. R. Brydon, D. F. Agterberg, M. Brando, and E. Hassinger Phys. Rev. X **12**, 031001 (2022).
- [40] Supplemental Material at XXX for the detailed discussion on the locally noncentrosymmetric superconductor. We also describe the detailed derivation of the energy and wave function of the OCABSs in Eq. (6), the Green’s function in Eq. (12), the tunneling conductance in Eq. (14), and the band basis Hamiltonian in Eq. (18). In addition, we show the electron part of the spectral function of UTe₂ in the presence of the spin-orbit couplings.
- [41] M. J. Rice and E. J. Mele, Phys. Rev. Lett. **49**, 1455 (1982).
- [42] E. Prodan, Phys. Rev. B **80**, 125327 (2009).
- [43] G. F. Lange, A. Bouhon, and R.-J. Slager, Phys. Rev. Research **5**, 033013 (2023).
- [44] K.-S. Lin, G. Palumbo, Z. Guo, J. Blackburn, D. P. Shoemaker, F. Mahmood, Z. Wang, G. A. Fiete, B. J. Wieder, and B. Bradlyn, Nat. Commun. **15**, 550 (2024).
- [45] P. A. Lee and D. S. Fisher, Phys. Rev. Lett. **47**, 882 (1981).
- [46] T. Ando, Phys. Rev. B **44**, 8017 (1991).
- [47] T. H. Hsieh and L. Fu, Phys. Rev. Lett. **108**, 107005 (2012).
- [48] S. Ando, S. Ikegaya, S. Tamura, Y. Tanaka, and K. Yada, Phys. Rev. B **106**, 214520 (2022).
- [49] Y. Fukaya, K. Yada, Y. Tanaka, P. Gentile, and M. Cuoco, Phys. Rev. B **108**, L020502 (2023).
- [50] G. E. Blonder, M. Tinkham, and T. M. Klapwijk, Phys. Rev. B **25**, 4515 (1982).
- [51] J. Nilsson, A. R. Akhmerov, and C. W. J. Beenakker, Phys. Rev. Lett. **101**, 120403 (2008).
- [52] J. Danon, A. B. Hellenes, E. B. Hansen, L. Casparis, A. P. Higginbotham, and K. Flensberg, Phys. Rev. Lett. **124**, 036801 (2020).
- [53] E. Dagotto, J. Riera, and D. Scalapino, Phys. Rev. B **45**, 5744(R) (1992).
- [54] T. M. Rice, S. Gopalan, and M. Sigrist, Europhys. Lett. **23**, 445 (1993).
- [55] E. Dagotto and T. M. Rice, Science **271**, 618 (1996).
- [56] M. Uehara, T. Nagata, J. Akimitsu, H. Takahashi, N. Môri, and K. Kinoshita, J. Phys. Soc. Jpn. **65**, 2764 (1996).
- [57] K. Kuroki, T. Higashida, and R. Arita, Phys. Rev. B **72**, 212509 (2005).
- [58] T. Vuletić, B. Korin-Hamzić, T. Ivek, S. Tomić, B. Gor-

- shunov, M. Dressel, and J. Akimitsu, Phys. Rep. **428**, 169 (2006).
- [59] H. Takahashi, A. Sugimoto, Y. Nambu, T. Yamauchi, Y. Hirata, T. Kawakami, M. Avdeev, K. Matsubayashi, F. Du, C. Kawashima, H. Soeda, S. Nakano, Y. Uwatoko, Y. Ueda, T. J. Sato, and K. Ohgushi, Nat. Mater. **14**, 1008 (2015).
- [60] H. Sakamoto and K. Kuroki Phys. Rev. Research **2**, 022055(R) (2020).
- [61] N. Bulut, D. J. Scalapino, and R. T. Scalettar, Phys. Rev. B **45**, 5577 (1992).
- [62] Richard T. Scalettar, Joel W. Cannon, Douglas J. Scalapino, and Robert L. Sugar, Phys. Rev. B **50**, 13419 (1994).
- [63] R. E. Hetzel, W. von der Linden, and W. Hanke, Phys. Rev. B **50**, 4159 (1994).
- [64] K. Kuroki, T. Kimura, and R. Arita, Phys. Rev. B **66**, 184508 (2002).
- [65] T. A. Maier and D. J. Scalapino, Phys. Rev. B **84**, 180513(R) (2011).
- [66] M. Nakata, D. Ogura, H. Usui, and K. Kuroki, Phys. Rev. B **95**, 214509 (2017).
- [67] H. Sun, M. Huo, X. Hu, J. Li, Z. Liu, Y. Han, L. Tang, Z. Mao, P. Yang, B. Wang, J. Cheng, D.-X. Yao, G.-M. Zhang, and M. Wang, Nature **621**, 493 (2023).
- [68] H. Sakakibara, M. Ochi, H. Nagata, Y. Ueki, H. Sakurai, R. Matsumoto, K. Terashima, K. Hirose, H. Ohta, M. Kato, Y. Takano, and K. Kuroki, arXiv:2309.09462 (2023).

Supplemental Material for ‘‘Oscillating-charged Andreev Bound States and Their Appearance in UTe₂’’

Satoshi Ando¹, Shingo Kobayashi², Andreas P. Schnyder³, Yasuhiro Asano⁴, and Satoshi Ikegaya^{1,5}

¹*Department of Applied Physics, Nagoya University, Nagoya 464-8603, Japan*

²*RIKEN Center for Emergent Matter Science, Wako, Saitama, 351-0198, Japan*

³*Max-Planck-Institut für Festkörperforschung, Heisenbergstrasse 1, D-70569 Stuttgart, Germany*

⁴*Department of Applied Physics, Hokkaido University, Sapporo 060-8628, Japan*

⁵*Institute for Advanced Research, Nagoya University, Nagoya 464-8601, Japan*

OSCILLATING-CHARGED ANDREEV BOUND STATES IN LOCALLY NONCENTROSYMMETRIC SUPERCONDUCTORS

In this section, we show the appearance of the oscillating-charged Andreev bound state (OCABS) in a locally noncentrosymmetric superconductor. The Bogoliubov–de Gennes (BdG) Hamiltonian of a locally noncentrosymmetric superconductor with an inter-layer pairing, which is proposed in Refs. [36, 37], is given by

$$\begin{aligned}
H &= \frac{1}{2} \sum_{\mathbf{k}, \sigma} [\psi_{\mathbf{k}\sigma}^\dagger, \psi_{-\mathbf{k}\bar{\sigma}}^\dagger] H_{\mathbf{k}} \begin{bmatrix} \psi_{\mathbf{k}\sigma} \\ \psi_{-\mathbf{k}\bar{\sigma}}^* \end{bmatrix} + H_{\text{soc}}, \\
\psi_{\mathbf{k}\sigma}^\dagger &= [\psi_{\mathbf{k}, \sigma, a, 1}^\dagger, \psi_{\mathbf{k}, \sigma, a, 2}^\dagger, \psi_{\mathbf{k}, \sigma, b, 1}^\dagger, \psi_{\mathbf{k}, \sigma, b, 2}^\dagger], \\
H_{\mathbf{k}} &= \begin{bmatrix} \tilde{h}(\mathbf{k}) & \tilde{h}_\Delta(\mathbf{k}) \\ \tilde{h}_\Delta^\dagger(\mathbf{k}) & -\tilde{h}^*(-\mathbf{k}) \end{bmatrix}, \\
\tilde{h}(\mathbf{k}) &= \begin{bmatrix} \hat{K}_{\mathbf{k}} & \hat{T}_{\mathbf{k}}^\dagger \\ \hat{T}_{\mathbf{k}} & \hat{K}_{\mathbf{k}} \end{bmatrix}, \\
\hat{K}_{\mathbf{k}} &= \begin{bmatrix} h_{00}(\mathbf{k}) & 0 \\ 0 & h_{00}(\mathbf{k}) \end{bmatrix}, \quad \hat{T}_{\mathbf{k}} = e^{i\frac{k_x}{2}} e^{i\frac{k_y}{2}} e^{i\frac{k_z}{2}} \begin{bmatrix} 0 & h_{10}(\mathbf{k}) - ih_{20}(\mathbf{k}) \\ h_{10}(\mathbf{k}) + ih_{20}(\mathbf{k}) & 0 \end{bmatrix}, \\
h_{00}(\mathbf{k}) &= 2t_p [\cos(k_x) + t_2 \cos(k_y)] - \mu, \\
h_{10}(\mathbf{k}) &= 4(t_u + t_d) \cos(k_x/2) \cos(k_y/2) \cos(k_z/2), \\
h_{20}(\mathbf{k}) &= -4(t_u - t_d) \cos(k_x/2) \cos(k_y/2) \sin(k_z/2), \\
\tilde{h}_\Delta(\mathbf{k}) &= \begin{bmatrix} 0 & \hat{\Delta}(\mathbf{k}) \\ \hat{\Delta}^\dagger(\mathbf{k}) & 0 \end{bmatrix}, \quad \hat{\Delta} = e^{i\frac{k_x}{2}} e^{i\frac{k_y}{2}} e^{i\frac{k_z}{2}} \begin{bmatrix} 0 & d_{13}(\mathbf{k}) \\ d_{13}(\mathbf{k}) & 0 \end{bmatrix}, \\
d_{13}(\mathbf{k}) &= \Delta \cos(k_x/2) \cos(k_y/2) \sin(k_z/2), \\
H_{\text{soc}} &= \frac{1}{2} \sum_{\mathbf{k}} [\psi_{\mathbf{k}\uparrow}^\dagger, \psi_{\mathbf{k}\downarrow}^\dagger, \psi_{-\mathbf{k}\uparrow}^\dagger, \psi_{-\mathbf{k}\downarrow}^\dagger] \Lambda_{\mathbf{k}} \begin{bmatrix} \psi_{\mathbf{k}\uparrow} \\ \psi_{\mathbf{k}\downarrow} \\ \psi_{-\mathbf{k}\uparrow}^* \\ \psi_{-\mathbf{k}\downarrow}^* \end{bmatrix}, \\
\Lambda_{\mathbf{k}} &= \begin{bmatrix} \lambda_{\mathbf{k}} & 0 \\ 0 & -\lambda_{-\mathbf{k}}^* \end{bmatrix}, \quad \lambda_{\mathbf{k}} = \begin{bmatrix} \tilde{\lambda}_{33}(\mathbf{k}) & \tilde{\lambda}_{31}(\mathbf{k}) - i\tilde{\lambda}_{32}(\mathbf{k}) \\ \tilde{\lambda}_{31}(\mathbf{k}) + i\tilde{\lambda}_{32}(\mathbf{k}) & -\tilde{\lambda}_{33}(\mathbf{k}) \end{bmatrix}, \\
\tilde{\lambda}_{3\nu}(\mathbf{k}) &= \begin{bmatrix} \hat{\lambda}_{3\nu}(\mathbf{k}) & 0 \\ 0 & \hat{\lambda}_{3\nu}(\mathbf{k}) \end{bmatrix}, \quad \hat{\lambda}_{3\nu}(\mathbf{k}) = \begin{bmatrix} h_{3\nu}(\mathbf{k}) & 0 \\ 0 & -h_{3\nu}(\mathbf{k}) \end{bmatrix}, \\
h_{31}(\mathbf{k}) &= -\alpha \sin(k_y), \quad h_{32}(\mathbf{k}) = \alpha \sin(k_x), \quad h_{33}(\mathbf{k}) = \lambda \sin(k_x) \sin(k_y) \sin(k_z) [\cos(k_x) - \cos(k_y)],
\end{aligned} \tag{22}$$

where $\psi_{\mathbf{k}, \sigma, \alpha, l}$ is the annihilation operator of an electron with momentum \mathbf{k} with spin σ at the l -th layer of the sublattice α . The index $\bar{\sigma}$ means the opposite spin of σ . Each hopping term is schematically illustrated in Fig. 4. The strength of the Rashba (Ising-type) spin-orbit coupling are described by α (λ). Note that Eq. (22) is modified to take into account the sublattice degrees of freedom explicitly. We assume the inter-layer-even spin-triplet odd-parity pair potential [36, 37]. When we neglect inter-layer hopping terms and the spin-orbit coupling terms, i.e.,

$$h_{10}(\mathbf{k}) = h_{20}(\mathbf{k}) = h_{31}(\mathbf{k}) = h_{32}(\mathbf{k}) = h_{33}(\mathbf{k}) = 0, \tag{23}$$

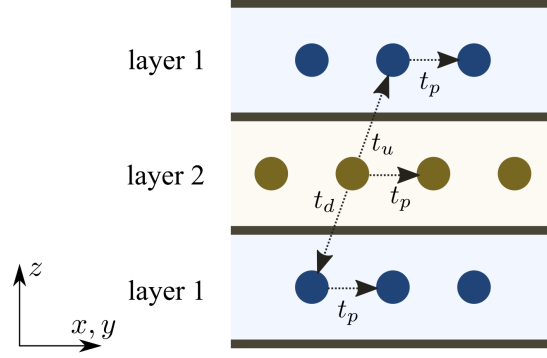


FIG. 4. Schematic image of the hopping terms.

the BdG Hamiltonian is rewritten as

$$\begin{aligned}
 H &= \frac{1}{2} \sum_{\mathbf{k}, \sigma, l} [\Psi_{\mathbf{k}, \sigma, l, +}^\dagger, \Psi_{\mathbf{k}, \sigma, l, -}^\dagger] \begin{bmatrix} h_{\mathbf{k}, +} & 0 \\ 0 & h_{\mathbf{k}, -} \end{bmatrix} \begin{bmatrix} \Psi_{\mathbf{k}, \sigma, l, +} \\ \Psi_{\mathbf{k}, \sigma, l, -} \end{bmatrix}, \\
 h_{\mathbf{k}, s} &= \begin{bmatrix} t_p \cos(k_x) - \mu(k_y) & \Delta_s(k_y, k_z) e^{-is\frac{k_x}{2}} \cos(k_x/2) \\ \Delta_s^*(k_y, k_z) e^{is\frac{k_x}{2}} \cos(k_x/2) & -t_p \cos(k_x) + \mu(k_y) \end{bmatrix}, \\
 \mu(k_y) &= \mu - t_p \cos(k_y), \quad \Delta_s(k_y, k_z) = \Delta e^{-is\frac{k_y}{2}} e^{-is\frac{k_z}{2}} \cos(k_y/2) \sin(k_z/2), \\
 \Psi_{\mathbf{k}, \sigma, l, +} &= [\psi_{\mathbf{k}, \sigma, a, l}, \psi_{-\mathbf{k}, \sigma, b, l}^\dagger]^\top, \quad \Psi_{\mathbf{k}, \sigma, l, -} = [\psi_{\mathbf{k}, \sigma, b, l}, \psi_{-\mathbf{k}, \sigma, a, l}^\dagger]^\top,
 \end{aligned} \tag{24}$$

where $s = +1$ (-1) and \bar{l} indicates the opposite layer of l . With fixed k_y and k_z , $h_{\mathbf{k}, s}$ coincides with the BdG Hamiltonian of the minimal model in Eq. (1) of the main text. Therefore, we can expect the appearance of the OCABSs in the locally noncentrosymmetric superconductor with the inter-layer pairing.

To demonstrate the appearance of the OCABSs, we consider the electron part of the spectral function, which is defined by

$$\rho_e(\tilde{x}, E) = \sum_{k_y, k_z} \rho_e(\tilde{x}, k_y, k_z, E), \tag{25}$$

$$\rho_e(\tilde{x}, k_y, k_z, E) = -\frac{1}{\pi} \text{Im}[g_{k_y, k_z}(\tilde{x}, \tilde{x}, E)], \tag{26}$$

where $\tilde{x} = x$ or $x + \frac{1}{2}$ measures the distant from the surface with x being integer numbers, and $g_{k_y, k_z}(\tilde{x}, \tilde{x}, E)$ is the retarded Green's function obtained using the recursive Green's function techniques [45, 46]. In Figs. 5(a) and 5(b), we show $\rho_e(\tilde{x}, E)$ at the outermost site ($\tilde{x} = 1$) and the second-outermost site ($\tilde{x} = 1 + \frac{1}{2}$) as a function of the energy, respectively. We assume the dominant inter-layer hopping case, i.e., $t_u, t_d > \alpha$. Specifically, we choose $(\mu, t_p, t_u, t_d, \alpha, \lambda, \Delta) = (0, 1, 0.2, 0.2, 0.05, 0, 0.001)$. Here we ignore the Ising-type spin-orbit coupling due to the inter-layer long-ranged hopping. In Figs. 6(a) and 6(b), we show $\rho_e(\tilde{x}, E)$ with the dominant Rashba spin-orbit coupling case, i.e., $t_u, t_d < \alpha$. Specifically, we choose $(\mu, t_p, t_u, t_d, \alpha, \lambda, \Delta) = (0, 1, 0.05, -0.05, 0.2, 0, 0.001)$. As shown in Fig. 5 and Fig. 6, in both cases, $\rho_e(\tilde{x}, E)$ at the outermost (second-outermost) has the significant peak only for $E < 0$ ($E > 0$). Thus, we confirm the appearance of the OCABSs in the locally noncentrosymmetric superconductor with the inter-layer pairing.

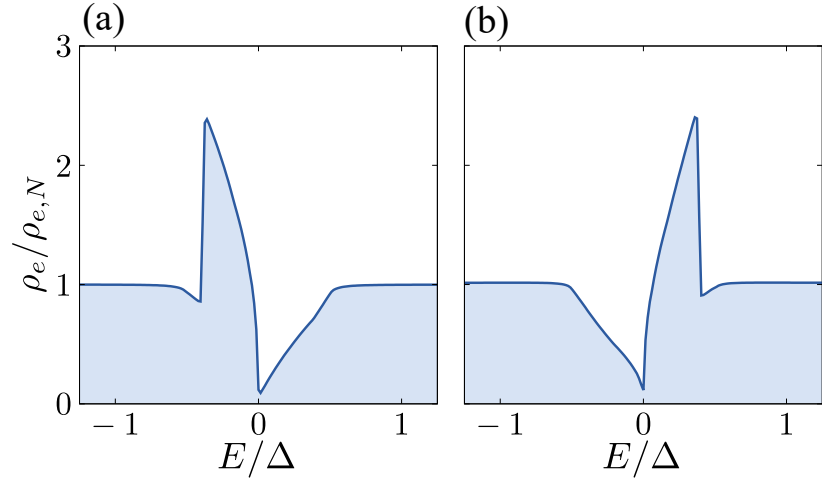


FIG. 5. Electron part of the spectral function with the dominant inter-layer hopping case (i.e., $t_u, t_d > \alpha$) as a function of the energy E . In (a), we show the result for the outermost site, i.e., $\tilde{x} = 1$, and in (b), we plot the result for the second-outermost site $\tilde{x} = 1 + \frac{1}{2}$.

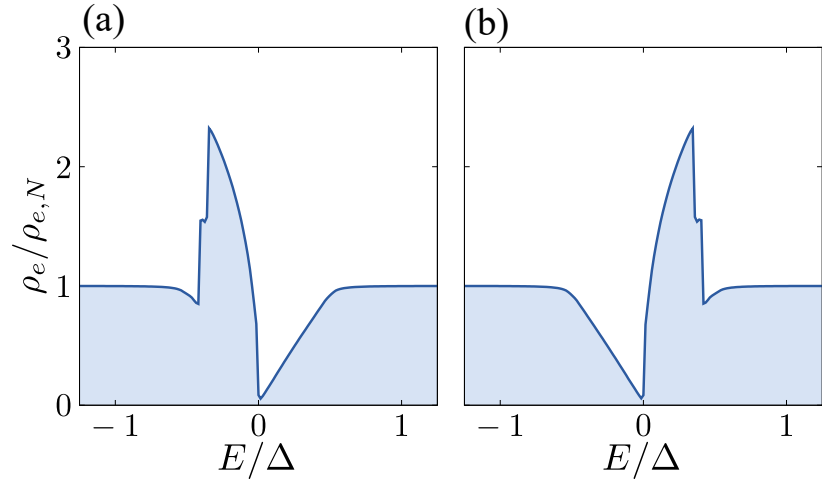


FIG. 6. Electron part of the spectral function with the dominant Rashba spin-orbit coupling case (i.e., $t_u, t_d < \alpha$) as a function of the energy E . In (a), we show the result for the outermost site, i.e., $\tilde{x} = 1$, and in (b), we plot the result for the second-outermost site $\tilde{x} = 1 + \frac{1}{2}$.

**ENERGY EIGENVALUE AND WAVE FUNCTION
OF THE OSCILLATING-CHARGED ANDREEV BOUND STATE**

In this section, we calculate the energy eigenvalue and the wave function of the OCABS in the minimal model. We consider the BdG equation, which is equivalent to Eq. (4) in the main text:

$$T_s \varphi_{x-1,s} + T_s^\dagger \varphi_{x+1,s} + K \varphi_{x,s} = E_s \varphi_{x,s}, \quad (27)$$

with

$$\begin{aligned} T_s &= \begin{bmatrix} \frac{t}{2} & \frac{(1+s)\Delta}{4} \\ \frac{(1-s)\Delta}{4} & -\frac{t}{2} \end{bmatrix}, \quad K = \begin{bmatrix} -\mu & \frac{\Delta}{2} \\ \frac{\Delta}{2} & \mu \end{bmatrix}, \\ \varphi_{x,+} &= [u_{x,+}, v_{x+\frac{1}{2},+}]^T, \quad \varphi_{x,-} = [u_{x+\frac{1}{2},-}, v_{x,-}]^T, \\ u_{x+\frac{1}{2},+} &= v_{x,+} = u_{x,-} = v_{x+\frac{1}{2},-} = 0, \end{aligned} \quad (28)$$

where $u_{x,s}$ ($v_{x,s}$) denotes the electron (hole) component in the a -sublattice, and $u_{x+\frac{1}{2},s}$ ($v_{x+\frac{1}{2},s}$) represents the electron (hole) component in the b -sublattice. We consider the semi-infinite system for $x > 0$ and apply an open-boundary condition, $\varphi_{0,s} = 0$.

We first focus on the solution belonging to $s = +$. Substituting

$$\varphi_{x,+} = \begin{bmatrix} u_{x,+} \\ v_{x+\frac{1}{2},+} \end{bmatrix} = \begin{bmatrix} u_k \\ v_k \end{bmatrix} e^{ikx}, \quad (29)$$

into Eq. (27), we obtain:

$$\begin{bmatrix} t \cos k - \mu & e^{-ik/2} \Delta \cos(k/2) \\ e^{ik/2} \Delta \cos(k/2) & -t \cos k + \mu \end{bmatrix} \begin{bmatrix} u_k \\ v_k \end{bmatrix} = E \begin{bmatrix} u_k \\ v_k \end{bmatrix}. \quad (30)$$

From Eq. (30), we find

$$E = \pm \sqrt{(t \cos(k) - \mu)^2 + \Delta^2 \cos^2(k/2)}, \quad (31)$$

and

$$\begin{bmatrix} u_k \\ v_k \end{bmatrix} \propto \begin{bmatrix} E + (t \cos(k) - \mu) \\ e^{ik/2} \Delta \cos(k/2) \end{bmatrix} \propto \begin{bmatrix} e^{-ik/2} \Delta \cos(k/2) \\ E - (t \cos(k) - \mu) \end{bmatrix}. \quad (32)$$

To investigate the Andreev bound states, we assume

$$k = q + i\kappa \quad (33)$$

where q and κ are real numbers. By substituting Eq. (33) into Eq. (31), we obtain

$$\begin{aligned} E^2 &= t^2 (\cos^2(q) \cosh^2(\kappa) - \sin^2(q) \sinh^2(\kappa)) - 2t\mu \cos(q) \cosh(\kappa) + \mu^2 + \Delta^2 \frac{1 + \cos(q) \cosh(\kappa)}{2} \\ &+ i \left(-2t^2 \cos(q) \cosh(\kappa) \sin(q) \sinh(\kappa) + 2t\mu \sin(q) \sinh(\kappa) - \Delta^2 \frac{\sin(q) \sinh(\kappa)}{2} \right). \end{aligned} \quad (34)$$

From the imaginary part of Eq. (34), we obtain

$$\cos(q) \cosh(\kappa) = \frac{4t\mu - \Delta^2}{4t^2}. \quad (35)$$

From the real part of Eq. (34) and Eq. (35), we obtain

$$\sin^2(q) \sinh^2(\kappa) = \frac{8t\mu\Delta^2 - \Delta^4 + 8t^2\Delta^2 - 16t^2E^2}{16t^4}. \quad (36)$$

Here we assume $\Delta/t \ll 1$ and approximate Eq. (35) and Eq. (36) as

$$\cos(q) \cosh(\kappa) = \frac{\mu}{t}, \quad (37)$$

$$\sin^2(q) \sinh^2(\kappa) = \frac{t\mu\Delta^2 + t^2\Delta^2 - 2t^2E^2}{2t^4}, \quad (38)$$

respectively. In general, the decay length of the Andreev bound state increases (i.e., κ decreases) by decreasing Δ . Thus, in the limit of $\Delta/t \ll 1$, we can expect $\kappa \ll 1$. On the basis of this expectation, we approximate Eq. (37) and Eq. (40) as

$$\cos(q) = \frac{\mu}{t}, \quad (39)$$

$$\kappa^2 \sin^2(q) = \frac{t\mu\Delta^2 + t^2\Delta^2 - 2t^2E^2}{2t^4}, \quad (40)$$

respectively. The expectation of $\kappa \ll 1$ is justified later. From Eq. (39), we obtain

$$q = \pm q_F, \quad q_F = \arccos\left(\frac{\mu}{t}\right), \quad (41)$$

where $-1 < \mu/t < 1$ is satisfied. From Eq. (40) and Eq. (41), we obtain

$$\kappa = \pm \kappa_E, \quad \kappa_E = \sqrt{\frac{t\mu\Delta^2 + t^2\Delta^2 - 2t^2E^2}{2t^2(t^2 - \mu^2)}}. \quad (42)$$

As a result, the wave function of the Andreev bound state is represented by

$$\varphi_{x,+} = a \begin{bmatrix} E + (t \cos(k_+) - \mu) \\ e^{ik_+/2} \Delta \cos(k_+/2) \end{bmatrix} e^{ik_+x} + b \begin{bmatrix} e^{ik_-/2} \Delta \cos(k_-/2) \\ E - (t \cos(k_-) - \mu) \end{bmatrix} e^{-ik_-x}, \quad (43)$$

$$k_{\pm} = q_F \pm i\kappa_E \quad (44)$$

where a and b are numerical coefficients. The wave function of $\varphi_{x,+}$ satisfies

$$\lim_{x \rightarrow \infty} \varphi_{x,+} = 0. \quad (45)$$

From the conditions of $\Delta/t \ll 1$ and $\kappa \ll 1$, we can approximate

$$\varphi_{x,+} \approx a \begin{bmatrix} E - it \sin(q_F) \kappa_E \\ e^{iq_F/2} \Delta \cos(q_F/2) \end{bmatrix} e^{ik_+x} + b \begin{bmatrix} e^{iq_F/2} \Delta \cos(q_F/2) \\ E - it \sin(q_F) \kappa_E \end{bmatrix} e^{-ik_-x}. \quad (46)$$

From the boundary condition of $\varphi_{x=0,+} = 0$, we obtain

$$\begin{bmatrix} E - it \sin(q_F) \kappa_E & e^{iq_F/2} \Delta \cos(q_F/2) \\ e^{iq_F/2} \Delta \cos(q_F/2) & E - it \sin(q_F) \kappa_E \end{bmatrix} \begin{bmatrix} a \\ b \end{bmatrix} = 0, \quad (47)$$

which leads

$$\begin{vmatrix} E - it \sin(q_F) \kappa_E & e^{iq_F/2} \Delta \cos(q_F/2) \\ e^{iq_F/2} \Delta \cos(q_F/2) & E - it \sin(q_F) \kappa_E \end{vmatrix} = 0. \quad (48)$$

By solving Eq. (48), we obtain the energy eigenvalue of the Andreev bound state as

$$E = E_+ = -\Delta \frac{t + \mu}{2t}. \quad (49)$$

By substituting Eq. (49) into Eq. (42), we find

$$\kappa_E = \kappa_0 = \frac{\Delta}{2t}, \quad (50)$$

which satisfies $\kappa_0 \ll 1$ for $\Delta/t \ll 1$. By substituting Eq. (49) into Eq. (47), we obtain

$$\begin{bmatrix} 1 & -1 \\ -1 & 1 \end{bmatrix} \begin{bmatrix} a \\ b \end{bmatrix} = 0, \quad (51)$$

which leads $a = b$. As a result, we find

$$\varphi_{x,+} = a \left(\begin{bmatrix} 1 \\ -1 \end{bmatrix} e^{ik_+x} + \begin{bmatrix} -1 \\ 1 \end{bmatrix} e^{-ik_-x} \right) = 2ia \begin{bmatrix} 1 \\ -1 \end{bmatrix} \sin(q_F x) e^{-\kappa_0 x}. \quad (52)$$

From the normalization condition,

$$\sum_x |\varphi_{x,+}|^2 = 1, \quad (53)$$

we obtain

$$\varphi_{x,+} = \begin{bmatrix} 1 \\ -1 \end{bmatrix} \phi_x, \quad \phi_x = \sqrt{2\kappa_0} \sin(q_F x) e^{-\kappa_0 x}. \quad (54)$$

The energy eigenvalue in Eq. (49) and the wave function in Eq. (54) are equivalent to those in Eq. (6) in the main text. In a similar manner, the energy eigenvalue and the wave function of the Andreev bound states belonging to $s = -$ are obtained as

$$E_- = \Delta \frac{t + \mu}{2t}, \quad \varphi_{x,-} = \begin{bmatrix} 1 \\ 1 \end{bmatrix} \phi_x, \quad (55)$$

respectively.

GREEN'S FUNCTION AT $E \approx E_{\pm}$

In this section, we calculate the retarded Green's function at $E \approx E_{\pm}$, which is given by Eq. (12) in the main text. At first, we consider the field operator

$$\Psi_{x,s} = \Psi_{x,s}^c + \Psi_{x,s}^a, \quad (56)$$

$$\Psi_{x,+} = \begin{bmatrix} \psi_x \\ \psi_{x+\frac{1}{2}}^\dagger \end{bmatrix}, \quad \Psi_{x,-} = \begin{bmatrix} \psi_{x+\frac{1}{2}} \\ \psi_x^\dagger \end{bmatrix}, \quad (57)$$

where $\psi_{\tilde{x}}$ ($\psi_{\tilde{x}}^\dagger$) with $\tilde{x} = x$ or $x + \frac{1}{2}$ represents the annihilation (creation) operator of the electron at \tilde{x} . The contribution from the continuum states to the field operator is given by

$$\Psi_{x,s}^c = \sum_{\nu} \left(\varphi_{x,s,\nu} \gamma_{s,\nu} + \bar{\varphi}_{x,s,\nu} \gamma_{-s,\nu}^\dagger \right), \quad (58)$$

$$(59)$$

where $\varphi_{x,s,\nu}$ satisfies

$$T_s \varphi_{x-1,s,\nu} + T_s^\dagger \varphi_{x+1,s,\nu} + K \varphi_{x,s,\nu} = E_{s,\nu} \varphi_{x,s,\nu}, \quad (60)$$

with $E_{s,\nu} > 0$ and

$$\lim_{x \rightarrow \infty} \psi_{x,s,\nu} \neq 0. \quad (61)$$

The wave function of $\bar{\varphi}_{x,s,\nu}$ is given by

$$\bar{\varphi}_{x,s,\nu} = C \varphi_{x,-s,\nu}, \quad C = \begin{bmatrix} 0 & 1 \\ -1 & 0 \end{bmatrix} \mathcal{K} \quad (62)$$

with \mathcal{K} being the complex conjugation operator, where $\bar{\varphi}_{x,s,\nu}$ satisfies

$$T_s \bar{\varphi}_{x-1,s,\nu} + T_s^\dagger \bar{\varphi}_{x+1,s,\nu} + K \bar{\varphi}_{x,s,\nu} = -E_{-s,\nu} \bar{\varphi}_{x,s,\nu}. \quad (63)$$

The annihilation (creation) operator of the Bogoliubov quasiparticle is given by $\gamma_{s,\nu}$ ($\gamma_{s,\nu}^\dagger$). The contribution from the Andreev bound state to the field operator is given by

$$\Psi_{x,s}^a = \begin{bmatrix} 1 \\ -s \end{bmatrix} \phi_x \gamma_{s,a} \quad (64)$$

where $\gamma_{s,a}$ denotes the annihilation operator of the Andreev bound state. The retarded Green's function is defined by

$$\begin{aligned} G_+(x, t; x', t') &= \begin{bmatrix} g(x, t; x', t') & f(x, t; x' + \frac{1}{2}, t') \\ \underline{f}(x + \frac{1}{2}, t; x', t') & \underline{g}(x + \frac{1}{2}, t; x' + \frac{1}{2}, t') \end{bmatrix} \\ &= -i\Theta(t - t') \begin{bmatrix} \{\psi_x(t), \psi_{x'}^\dagger(t')\} & \{\psi_x(t), \psi_{x+\frac{1}{2}}(t')\} \\ \{\psi_{x+\frac{1}{2}}^\dagger(t), \psi_x^\dagger(t')\} & \{\psi_{x+\frac{1}{2}}^\dagger(t), \psi_{x+\frac{1}{2}}(t')\} \end{bmatrix}, \end{aligned} \quad (65)$$

$$\begin{aligned} G_-(x, t; x', t') &= \begin{bmatrix} g(x + \frac{1}{2}, t; x' + \frac{1}{2}, t') & f(x + \frac{1}{2}, t; x', t') \\ \underline{f}(x, t; x' + \frac{1}{2}, t') & \underline{g}(x, t; x', t') \end{bmatrix} \\ &= -i\Theta(t - t') \begin{bmatrix} \{\psi_{x+\frac{1}{2}}(t), \psi_{x'+\frac{1}{2}}^\dagger(t')\} & \{\psi_{x+\frac{1}{2}}(t), \psi_x(t')\} \\ \{\psi_x^\dagger(t), \psi_{x+\frac{1}{2}}^\dagger(t')\} & \{\psi_x^\dagger(t), \psi_x(t')\} \end{bmatrix}, \end{aligned} \quad (66)$$

where

$$g(x, t; x' + \frac{1}{2}, t') = g(x + \frac{1}{2}, t; x', t') = \underline{g}(x, t; x' + \frac{1}{2}, t') = \underline{g}(x + \frac{1}{2}, t; x', t') = 0, \quad (67)$$

$$f(x, t; x', t') = f(x + \frac{1}{2}, t; x' + \frac{1}{2}, t') = \underline{f}(x, t; x', t') = \underline{f}(x + \frac{1}{2}, t; x' + \frac{1}{2}, t') = 0. \quad (68)$$

In the spectral representation, the retarded Green's function is given by

$$G_+(x, x', E) = \begin{bmatrix} g(x, x', E) & f(x, x' + \frac{1}{2}, E) \\ \underline{f}(x + \frac{1}{2}, x', E) & \underline{g}(x + \frac{1}{2}, x' + \frac{1}{2}, E) \end{bmatrix} = G_+^c(x, x', E) + G_+^a(x, x', E), \quad (69)$$

$$G_-(x, x', E) = \begin{bmatrix} g(x + \frac{1}{2}, x' + \frac{1}{2}, E) & f(x + \frac{1}{2}, x', E) \\ \underline{f}(x, x' + \frac{1}{2}, E) & \underline{g}(x, x', E) \end{bmatrix} = G_-^c(x, x', E) + G_-^a(x, x', E), \quad (70)$$

where

$$G_s^c(x, x', E) = \sum_\nu \left(\varphi_{x,s,\nu} \frac{1}{E - E_{s,\nu} + i\delta} \varphi_{x',s,\nu}^\dagger + \bar{\varphi}_{x,s,\nu} \frac{1}{E + E_{-s,\nu} + i\delta} \bar{\varphi}_{x',s,\nu}^\dagger \right), \quad (71)$$

$$G_s^a(x, x', E) = \frac{\phi_x \phi_{x'}}{E - E_s + i\delta} \begin{bmatrix} 1 & -s \\ -s & 1 \end{bmatrix}. \quad (72)$$

When we focus on $E \approx E_s$, the contribution from the continuum states to the Green's function, i.e., $G_s^c(x, x', E)$ is negligible. Therefore, we obtain

$$G_s(x, x', E) \approx G_s^a(x, x', E), \quad (73)$$

for $E \approx E_s$. As a result, we find

$$\begin{aligned} g(x, x, E) &= \underline{g}(x + \frac{1}{2}, x + \frac{1}{2}, E) = \frac{|\phi_x|^2}{E + E_c + i\delta}, \\ g(x + \frac{1}{2}, x + \frac{1}{2}, E) &= \underline{g}(x, x, E) = \frac{|\phi_x|^2}{E - E_c + i\delta}, \end{aligned} \quad (74)$$

with $E_c = |E_s|$, which is equivalent to Eq. (12) in the main text.

**DIFFERENTIAL CONDUCTANCE
IN THE PRESENCE OF ANDREEV BOUND STATES**

In this section, we derive the differential conductance given by Eq. (14) in the main text. We start with a tight-binding BdG Hamiltonian describing a normal-metal–superconductor junction,

$$H = H_S + H_N + H_T, \quad (75)$$

$$H_S = \sum_{x,x'>0} [c_x^\dagger, c_x] \begin{bmatrix} h(x, x') & \Delta(x, x') \\ -\Delta^*(x, x') & -h^*(x, x') \end{bmatrix} \begin{bmatrix} c_{x'} \\ c_{x'}^\dagger \end{bmatrix}, \quad (76)$$

$$H_N = -t \sum_{x<0} (a_{x+1}^\dagger a_x + \text{h.c.}), \quad (77)$$

$$H_T = -t'(c_{x=1}^\dagger a_{x=0} + \text{h.c.}), \quad (78)$$

where c_x (a_x) represents the annihilation operator of the electron in the superconducting (normal) segment. For the superconducting segment (i.e., $x > 0$), the kinetic energy in the normal state is described by $h(x, x')$, and the pair potential is given by $\Delta(x, x')$. The hopping integral in the normal segment ($x \leq 0$) is given by t . The hopping integral at the interface is represented by t' . The Bogoliubov transformation is denoted by

$$\begin{bmatrix} c_x \\ c_x^\dagger \end{bmatrix} = \sum_{\nu} \left(\begin{bmatrix} u_{\nu}(x) \\ v_{\nu}(x) \end{bmatrix} \gamma_{\nu} + \begin{bmatrix} v_{\nu}^*(x) \\ u_{\nu}^*(x) \end{bmatrix} \gamma_{\nu}^\dagger \right), \quad (79)$$

where

$$\sum_{x'>0} \begin{bmatrix} h(x, x') & \Delta(x, x') \\ -\Delta^*(x, x') & -h^*(x, x') \end{bmatrix} \begin{bmatrix} u_{\nu}(x') \\ v_{\nu}(x') \end{bmatrix} = E_{\nu} \begin{bmatrix} u_{\nu}(x) \\ v_{\nu}(x) \end{bmatrix}, \quad (x > 0) \quad (80)$$

and γ_{ν} (γ_{ν}^\dagger) represents the annihilation (creation) operator of a Bogoliubov quasiparticle having the energy E_{ν} . In what follows, we assume

$$0 < E_{\nu} < E_{\nu+1}. \quad (\nu \geq 1) \quad (81)$$

The BdG Hamiltonian H_S is rewritten as

$$H_S = \frac{1}{2} [\gamma^\dagger, \gamma^T] \mathcal{H} \begin{bmatrix} \gamma \\ \gamma^* \end{bmatrix}, \quad (82)$$

$$\gamma = [\gamma_1, \gamma_2, \dots, \gamma_i, \gamma_{i+1}, \dots]^T, \quad (83)$$

$$\mathcal{H} = \begin{bmatrix} \mathcal{E} & 0 \\ 0 & -\mathcal{E} \end{bmatrix}, \quad \mathcal{E} = \text{diag}[E_1, E_2, \dots, E_i, E_{i+1}, \dots]. \quad (84)$$

The tunneling Hamiltonian H_T is rewritten as

$$H_T = \frac{1}{2} \left([\gamma^\dagger, \gamma^T] \mathcal{W} \begin{bmatrix} a_0 \\ a_0^\dagger \end{bmatrix} + \text{h.c.} \right), \quad (85)$$

$$\mathcal{W} = \begin{bmatrix} \underline{W} \\ \underline{W} \end{bmatrix}, \quad \underline{W} = \begin{bmatrix} W_1 \\ W_2 \\ \vdots \\ W_i \\ W_{i+1} \\ \vdots \end{bmatrix}, \quad \underline{\underline{W}} = \begin{bmatrix} \underline{W}_1 \\ \underline{W}_2 \\ \vdots \\ \underline{W}_i \\ \underline{W}_{i+1} \\ \vdots \end{bmatrix}, \quad (86)$$

$$\underline{W}_{\nu} = [-t' u_{\nu}^*(1), t' v_{\nu}^*(1)], \quad \underline{\underline{W}}_{\nu} = [-t' v_{\nu}(1), t' u_{\nu}(1)]. \quad (87)$$

By using \mathcal{H} and \mathcal{W} , we can calculate the scattering matrix by [51, 52]

$$S(E) = \begin{bmatrix} s^{ee}(E) & s^{eh}(E) \\ s^{he}(E) & s^{hh}(E) \end{bmatrix} = 1 - 2 \frac{i}{t} \mathcal{W}^\dagger \left[E - \mathcal{H} + \frac{i}{t} \mathcal{W} \mathcal{W}^\dagger \right]^{-1} \mathcal{W}, \quad (88)$$

where s^{ee} and s^{he} (s^{eh} and s^{hh}) represents the scattering coefficients from the electron (hole) to the electron and hole, respectively.

We assume that the eigen states of $\nu = 1$ corresponds to the Andreev bound states having energy E_B (i.e., $E_1 = E_B$). Moreover, we assume that the Andreev bound states is energetically separated from other states as

$$E_2 - E_B \gg \frac{|t'u_\nu(1)|^2}{t}, \quad E_2 - E_B \gg \frac{|t'v_\nu(1)|^2}{t}, \quad (89)$$

and

$$2E_B \gg \frac{|t'u_\nu(1)|^2}{t}, \quad 2E_B \gg \frac{|t'v_\nu(1)|^2}{t}, \quad (90)$$

where Eq. (89) characterizes the energy difference between the Andreev bound state and the continuum states, and Eq. (90) characterizes the energy difference between the positive energy Andreev bound states and the negative energy Andreev bound states. The conditions of Eq. (89) and Eq. (90) can be satisfied with sufficiently low transparency junctions (i.e., $t'/t \ll 1$). When we focus on the scattering matrix at $E \approx E_B$, we can approximate [51, 52]

$$S(E) \approx 1 - 2\frac{i}{t}W_1^\dagger \left[E - E_B + \frac{i}{t}W_1W_1^\dagger \right]^{-1} W_1 = 1 - \frac{2i}{E - E_B + i(|U|^2 + |V|^2)} \begin{bmatrix} |U|^2 & -UV^* \\ -U^*V & |V|^2 \end{bmatrix}, \quad (91)$$

$$U = -\frac{t'u_1(1)}{\sqrt{t}}, \quad V = -\frac{t'v_1(1)}{\sqrt{t}}. \quad (92)$$

The differential conductance with the bias voltages below the superconducting gap is evaluated by

$$G(eV) = \frac{2e^2}{h} |s^{he}(E)|_{E=eV}^2. \quad (93)$$

Therefore, for $eV \approx E_B$, we obtain

$$G(eV) \approx \frac{e^2}{h} \frac{8(|U||V|)^2}{(eV - E_B)^2 + (|U|^2 + |V|^2)^2}, \quad (94)$$

which is equivalent to Eq. (14) in the main text.

In addition, we discuss the differential conductance in the presence of OCABSs. Here, we focus on the positive energy OCABS in the minimal model, where the energy eigen value and the wave function are given by

$$E_B = \Delta \frac{t + \mu}{2t}, \quad \begin{bmatrix} u_1(x + \frac{1}{2}) \\ v_1(x) \end{bmatrix} = \begin{bmatrix} 1 \\ 1 \end{bmatrix} \phi_x, \quad (95)$$

respectively, which are also given in Eq. (55) of this Supplemental Material. Since $|U|=0$ owing to $u_1(x=1)=0$, we obtain $G(eV \approx E_B) = 0$, where the absence of the conductance peak at $eV = E_B$ is also discussed in the main text.

SUPERCONDUCTOR UTe₂

Bogoliubov–de Gennes Hamiltonian including the spin-orbit coupling potential

In this section, we show the BdG Hamiltonian for the superconductor UTe₂, which is proposed in Ref. [25]:

$$\begin{aligned}
H_{\text{all}} &= H + H_{\text{soc}}, \\
H &= \frac{1}{2} \sum_{\mathbf{k}, \sigma} [\psi_{\mathbf{k}\sigma}^\dagger, \psi_{-\mathbf{k}\bar{\sigma}}^\dagger] H_{\mathbf{k}} \begin{bmatrix} \psi_{\mathbf{k}\sigma} \\ \psi_{-\mathbf{k}\bar{\sigma}}^* \end{bmatrix}, \\
\psi_{\mathbf{k}\sigma}^\dagger &= [\psi_{\mathbf{k}, \sigma, a, 1}^\dagger, \psi_{\mathbf{k}, \sigma, a, 2}^\dagger, \psi_{\mathbf{k}, \sigma, b, 1}^\dagger, \psi_{\mathbf{k}, \sigma, b, 2}^\dagger], \\
H_{\mathbf{k}} &= \begin{bmatrix} \tilde{h}_{\mathbf{k}} & \tilde{h}_{\Delta} \\ \tilde{h}_{\Delta}^\dagger & -\tilde{h}_{-\mathbf{k}}^* \end{bmatrix}, \\
\tilde{h}_{\mathbf{k}} &= \begin{bmatrix} \hat{K}_{\mathbf{k}} & \hat{T}_{\mathbf{k}}^\dagger \\ \hat{T}_{\mathbf{k}} & \hat{K}_{\mathbf{k}} \end{bmatrix}, \\
\hat{K}_{\mathbf{k}} &= \begin{bmatrix} \epsilon_{\mathbf{k}} & m_g \\ m_g & \epsilon_{\mathbf{k}} \end{bmatrix}, \quad \hat{T}_{\mathbf{k}} = e^{i\frac{k_x}{2}} e^{i\frac{k_y}{2}} e^{i\frac{k_z}{2}} \begin{bmatrix} 0 & f_{g, \mathbf{k}} - if_{z, \mathbf{k}} \\ f_{g, \mathbf{k}} + if_{z, \mathbf{k}} & 0 \end{bmatrix}, \\
\epsilon_{\mathbf{k}} &= t_1 \cos(k_x) + t_2 \cos(k_y) - \mu, \\
f_{g, \mathbf{k}} &= t_3 \cos(k_x/2) \cos(k_y/2) \cos(k_z/2), \\
f_{z, \mathbf{k}} &= t_z \cos(k_x/2) \cos(k_y/2) \sin(k_z/2), \\
\tilde{h}_{\Delta} &= \begin{bmatrix} \hat{\Delta} & 0 \\ 0 & \hat{\Delta} \end{bmatrix}, \quad \hat{\Delta} = \begin{bmatrix} 0 & \Delta \\ -\Delta & 0 \end{bmatrix},
\end{aligned} \tag{96}$$

where $\psi_{\mathbf{k}, \sigma, \alpha, l}$ is the annihilation operator of an electron with momentum \mathbf{k} with spin σ at the l -th rung of the sublattice α . The index $\bar{\sigma}$ means the opposite spin of σ . The each hopping term is schematically illustrated in Fig. 7. According to Ref. [25], we choose the fitting parameters as $(\mu, t_1, t_2, m_0, t_3, t_z) = (-0.129, -0.0892, 0.0678, -0.062, 0.0742, -0.0742)$. We assume the inter-rung-odd spin-triplet s -wave pair potential belonging to A_u symmetry, where

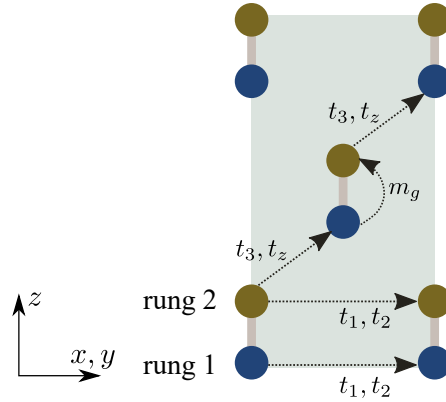


FIG. 7. Schematic image of the hopping terms.

we choose $\Delta = 0.001$. The spin-orbit coupling potential, which is ignored in the main text, is described by

$$H_{\text{soc}} = \frac{1}{2} \sum_{\mathbf{k}} [\psi_{\mathbf{k}\uparrow}^\dagger, \psi_{\mathbf{k}\downarrow}^\dagger, \psi_{-\mathbf{k}\uparrow}^\dagger, \psi_{-\mathbf{k}\downarrow}^\dagger] \Lambda_{\mathbf{k}} \begin{bmatrix} \psi_{\mathbf{k}\uparrow} \\ \psi_{\mathbf{k}\downarrow} \\ \psi_{-\mathbf{k}\uparrow}^* \\ \psi_{-\mathbf{k}\downarrow}^* \end{bmatrix}, \quad (97)$$

$$\Lambda_{\mathbf{k}} = \begin{bmatrix} \lambda_{\mathbf{k}} & 0 \\ 0 & -\lambda_{-\mathbf{k}}^* \end{bmatrix}, \quad \lambda_{\mathbf{k}} = \begin{bmatrix} \tilde{\lambda}_{\mathbf{k},z} & \tilde{\lambda}_{\mathbf{k},x} - i\tilde{\lambda}_{\mathbf{k},y} \\ \tilde{\lambda}_{\mathbf{k},x} + i\tilde{\lambda}_{\mathbf{k},y} & -\tilde{\lambda}_{\mathbf{k},z} \end{bmatrix}, \quad (98)$$

$$\tilde{\lambda}_{\mathbf{k},x(y)} = \begin{bmatrix} \hat{\lambda}_{\mathbf{k},x(y)} & 0 \\ 0 & \hat{\lambda}_{\mathbf{k},x(y)} \end{bmatrix}, \quad \hat{\lambda}_{\mathbf{k},x(y)} = \begin{bmatrix} t_{x(y)} \sin(k_{x(y)}) & 0 \\ 0 & -t_{x(y)} \sin(k_{x(y)}) \end{bmatrix}, \quad (99)$$

$$\tilde{\lambda}_{\mathbf{k},z} = \begin{bmatrix} 0 & \hat{\lambda}_{\mathbf{k},z}^\dagger \\ \hat{\lambda}_{\mathbf{k},z} & 0 \end{bmatrix}, \quad \hat{\lambda}_{\mathbf{k},z} = e^{i\frac{k_x}{2}} e^{i\frac{k_y}{2}} e^{i\frac{k_z}{2}} \begin{bmatrix} f_{u,\mathbf{k}} & 0 \\ 0 & -f_{u,\mathbf{k}} \end{bmatrix}, \quad (100)$$

$$f_{u,\mathbf{k}} = t_u \sin(k_x/2) \sin(k_y/2) \sin(k_z/2), \quad (101)$$

where $(t_x, t_y, t_u) = (0.006, 0.008, 0.01)$ [25].

In what follows, we focus on the Andreev bound states at the surface parallel to the x direction. The electron part of the spectral function is defined by

$$\rho_e(\tilde{y}, E) = \sum_{k_x, k_z} \rho_e(\tilde{y}, k_x, k_z, E), \quad (102)$$

$$\rho_e(\tilde{y}, k_x, k_z, E) = -\frac{1}{\pi} \text{Im}[g_{k_x, k_z}(\tilde{y}, \tilde{y}, E)], \quad (103)$$

where $\tilde{y} = y$ or $y + \frac{1}{2}$ measures the distant from the surface with y being integer numbers, and $g_{k_x, k_z}(\tilde{y}, \tilde{y}, E)$ is the retarded Green's function obtained using the recursive Green's function techniques [45, 46]. In Figs. 8(a), we show $\rho_e(\tilde{y}, E)$ at the outermost site ($\tilde{y} = 1$) and the second-outermost site ($\tilde{y} = 1 + \frac{1}{2}$) as a function of the energy, respectively. We find that $\rho_e(\tilde{y}, E)$ at the outermost (second-outermost) has the significant hump only for $E < 0$ ($E > 0$). As a result, we confirm the appearance of the OCABSs even with the spin-orbit coupling potentials.

Band basis Hamiltonian at $k_z = \pi$

In this section, we calculate the band-basis Hamiltonian at $k_z = \pi$, which is given by Eq. (18) in the main text. Here, we ignore the spin-orbit coupling H_{soc} . At $k_z = \pi$, the Hamiltonian $H_{\mathbf{k}}$ in Eq. (96) is rewritten as

$$H_{\mathbf{q}} = \begin{bmatrix} \tilde{h}_{\mathbf{q}} & \tilde{h}_{\Delta} \\ \tilde{h}_{\Delta}^\dagger & -\tilde{h}_{-\mathbf{q}}^* \end{bmatrix}, \quad (104)$$

$$\tilde{h}_{\mathbf{q}} = \begin{bmatrix} \epsilon_{\mathbf{q}} & m_{\mathbf{g}} & 0 & -\chi_{\mathbf{q}}^* f_{z,\mathbf{q}} \\ m_{\mathbf{g}} & \epsilon_{\mathbf{q}} & \chi_{\mathbf{q}}^* f_{z,\mathbf{q}} & 0 \\ 0 & \chi_{\mathbf{q}} f_{z,\mathbf{q}} & \epsilon_{\mathbf{q}} & m_{\mathbf{g}} \\ -\chi_{\mathbf{q}} f_{z,\mathbf{q}} & 0 & m_{\mathbf{g}} & \epsilon_{\mathbf{q}} \end{bmatrix}, \quad \chi_{\mathbf{q}} = e^{i\frac{k_x}{2}} e^{i\frac{k_y}{2}}, \quad (105)$$

where $\mathbf{q} = (k_x, k_y, k_z = \pi)$. By using a unitary operator,

$$U_A = U_4 U_3 U_2 U_1, \quad (106)$$

$$U_1 = \begin{bmatrix} \tilde{U}_1 & 0 \\ 0 & \tilde{U}_1 \end{bmatrix}, \quad \tilde{U}_1 = \frac{1}{\sqrt{2}} \begin{bmatrix} 1 & 1 & 0 & 0 \\ -1 & 1 & 0 & 0 \\ 0 & 0 & 1 & 1 \\ 0 & 0 & -1 & 1 \end{bmatrix}, \quad (107)$$

$$U_2 = \begin{bmatrix} \tilde{U}_2 & 0 \\ 0 & \tilde{U}_2 \end{bmatrix}, \quad \tilde{U}_2 = \begin{bmatrix} 1 & 0 & 0 & 0 \\ 0 & 0 & 0 & 1 \\ 0 & 1 & 0 & 0 \\ 0 & 0 & 1 & 0 \end{bmatrix}, \quad (108)$$

$$U_3 = \begin{bmatrix} \hat{1} & 0 & 0 & 0 \\ 0 & 0 & 0 & \hat{1} \\ 0 & \hat{1} & 0 & 0 \\ 0 & 0 & \hat{1} & 0 \end{bmatrix}, \quad \hat{1} = \begin{bmatrix} 1 & 0 \\ 0 & 1 \end{bmatrix}, \quad (109)$$

$$U_4 = \begin{bmatrix} \tilde{U}_4 & 0 \\ 0 & \tilde{U}_4 \end{bmatrix}, \quad \tilde{U}_4 = \begin{bmatrix} 1 & 0 & 0 & 0 \\ 0 & 1 & 0 & 0 \\ 0 & 0 & 0 & 1 \\ 0 & 0 & 1 & 0 \end{bmatrix}, \quad (110)$$

we deform the Hamiltonian $H_{\mathbf{q}}$ as

$$H'_{\mathbf{q}} = U_A H_{\mathbf{q}} U_A^\dagger = \begin{bmatrix} \check{H}'_{\mathbf{q},+} & 0 \\ 0 & \check{H}'_{\mathbf{q},-} \end{bmatrix}, \quad (111)$$

$$\check{H}'_{\mathbf{q},s} = \begin{bmatrix} \epsilon_{\mathbf{q}} + sm_g & -s\chi_{\mathbf{q}}^* f_{z,\mathbf{q}} & 0 & s\Delta \\ -s\chi_{\mathbf{q}} f_{z,\mathbf{q}} & \epsilon_{\mathbf{q}} - sm_g & -s\Delta & 0 \\ 0 & -s\Delta & -\epsilon_{\mathbf{q}} - sm_g & -s\chi_{\mathbf{q}} f_{z,\mathbf{q}} \\ s\Delta & 0 & -s\chi_{\mathbf{q}}^* f_{z,\mathbf{q}} & -\epsilon_{\mathbf{q}} + sm_g \end{bmatrix}. \quad (112)$$

Furthermore, by using a unitary operator,

$$U_5 = \begin{bmatrix} \check{U}_5 & 0 \\ 0 & \check{U}_5 \end{bmatrix}, \quad \check{U}_5 = \begin{bmatrix} \hat{U}_5 & 0 \\ 0 & \hat{U}_5 \end{bmatrix}, \quad (113)$$

$$\hat{U}_5 = \frac{1}{\sqrt{2V_{\mathbf{q}}(V_{\mathbf{q}} + m_g)}} \begin{bmatrix} V_{\mathbf{q}} + m_g & -\chi_{\mathbf{q}}^* f_{z,\mathbf{q}} \\ -\chi_{\mathbf{q}} f_{z,\mathbf{q}} & -(V_{\mathbf{q}} + m_g) \end{bmatrix}, \quad (114)$$

$$\hat{U}_5 = \frac{1}{\sqrt{2V_{\mathbf{q}}(V_{\mathbf{q}} + m_g)}} \begin{bmatrix} V_{\mathbf{q}} + m_g & \chi_{\mathbf{q}} f_{z,\mathbf{q}} \\ \chi_{\mathbf{q}}^* f_{z,\mathbf{q}} & -(V_{\mathbf{q}} + m_g) \end{bmatrix}, \quad (115)$$

$$V_{\mathbf{q}} = \sqrt{m_g^2 + f_{z,\mathbf{q}}^2}, \quad (116)$$

we eventually obtain the band-basis Hamiltonian,

$$H_{\mathbf{q}}^{\text{band}} = U_5 H'_{\mathbf{q}} U_5^\dagger = \begin{bmatrix} \check{H}_{\mathbf{q},+} & 0 \\ 0 & \check{H}_{\mathbf{q},-} \end{bmatrix} \quad (117)$$

$$\check{H}_{\mathbf{q},s} = \begin{bmatrix} \epsilon_{\mathbf{q}} + sV_{\mathbf{q}} & 0 & s\Delta\alpha_{\mathbf{q},-} & -s\Delta\beta_{\mathbf{q}} \\ 0 & \epsilon_{\mathbf{q}} - sV_{\mathbf{q}} & s\Delta\beta_{\mathbf{q}} & s\Delta\alpha_{\mathbf{q},+} \\ s\Delta\alpha_{\mathbf{q},+} & s\Delta\beta_{\mathbf{q}} & -\epsilon_{\mathbf{q}} - sV_{\mathbf{q}} & 0 \\ -s\Delta\beta_{\mathbf{q}} & s\Delta\alpha_{\mathbf{q},-} & 0 & -\epsilon_{\mathbf{q}} + sV_{\mathbf{q}} \end{bmatrix}, \quad (118)$$

$$\alpha_{\mathbf{q},\pm} = e^{\pm ik_x/2} e^{\pm ik_y/2} \frac{f_{z,\mathbf{q}}}{V_{\mathbf{q}}}, \quad \beta_{\mathbf{q}} = \frac{m_g}{V_{\mathbf{q}}}, \quad (119)$$

which is equivalent to Eq. (18) in the main text.

Electron part of spectral function with other pairing symmetries

In this section, we show the electron part of spectral function with other possible pairing symmetries discussed in Ref. [25]. Specifically, we consider the inter-rung-odd spin-triplet s -wave pair potential belonging to B_{2u} and B_{3u} symmetries. The BdG Hamiltonian is given by

$$\begin{aligned}
 H &= \frac{1}{2} \sum_{\mathbf{k}, \sigma} [\psi_{\mathbf{k}\sigma}^\dagger, \psi_{-\mathbf{k}\sigma}^\dagger] H_{\mathbf{k}}^{2u(3u)} \begin{bmatrix} \psi_{\mathbf{k}\sigma} \\ \psi_{-\mathbf{k}\sigma}^* \end{bmatrix} + H_{\text{soc}}, \\
 H_{\mathbf{k}}^{2u(3u)} &= \begin{bmatrix} \tilde{h}_{\mathbf{k}} & \tilde{h}_{\Delta, \sigma}^{2u(3u)} \\ \left\{ \tilde{h}_{\Delta, \sigma}^{2u(3u)} \right\}^\dagger & -\tilde{h}_{-\mathbf{k}}^* \end{bmatrix}, \\
 \tilde{h}_{\Delta, \sigma}^{2u} &= -s_\sigma \begin{bmatrix} \hat{\Delta} & 0 \\ 0 & \hat{\Delta} \end{bmatrix}, \quad \tilde{h}_{\Delta, \sigma}^{3u} = i \begin{bmatrix} \hat{\Delta} & 0 \\ 0 & \hat{\Delta} \end{bmatrix},
 \end{aligned} \tag{120}$$

where $s_{\uparrow(\downarrow)} = 1$ (-1). In what follows, we focus on the Andreev bound states at the surface parallel to the x direction. In Figs. 9(a) and 9(b), we show $\rho_e(\tilde{y}, E)$ with B_{2u} pairing symmetry at the outermost site ($\tilde{y} = 1$) and the second-outermost site ($\tilde{y} = 1 + \frac{1}{2}$) as a function of the energy, respectively. In Figs. 10(a) and 10(b), we show $\rho_e(\tilde{y}, E)$ with B_{3u} pairing symmetry at $\tilde{y} = 1$ and $\tilde{y} = 1 + \frac{1}{2}$ as a function of E , respectively. In both cases, we find that $\rho_e(\tilde{y}, E)$ at the outermost (second-outermost) has the significant hump only for $E < 0$ ($E > 0$). As a result, we confirm the appearance of the OCABSs even with B_{2u} and B_{3u} symmetries.

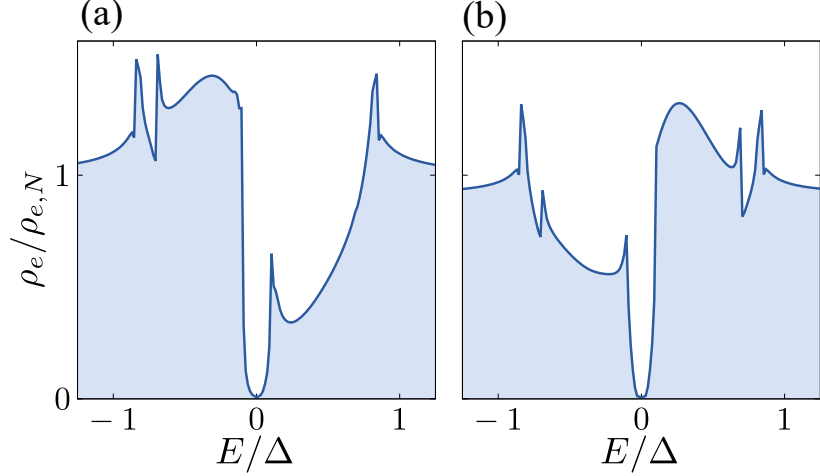


FIG. 8. Electron part of the spectral function in the presence of the spin-orbit coupling potentials as a function of the energy E . The pair potential is belonging to A_u pairing symmetry. In (a), we show the result for the outermost site, i.e., $\tilde{y} = 1$, and in (b), we plot the result for the second-outermost site $\tilde{y} = 1 + \frac{1}{2}$.

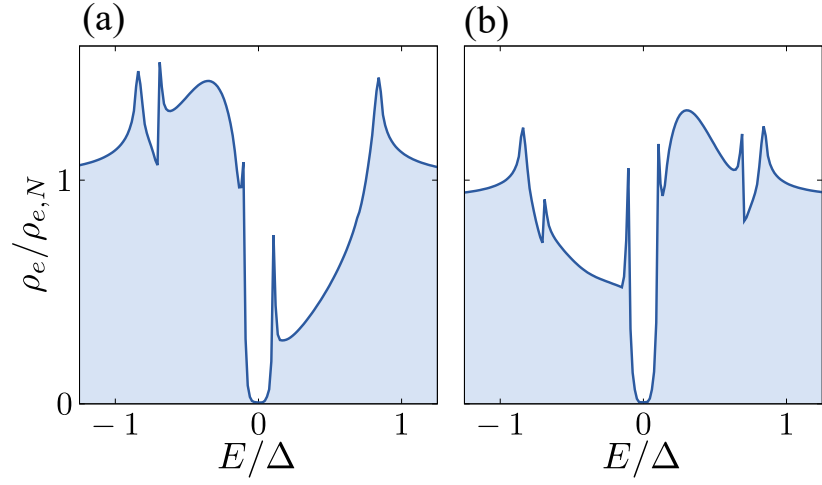


FIG. 9. Electron part of the spectral function with B_{2u} pairing symmetry as a function of the energy E . In (a), we show the result for the outermost site, i.e., $\tilde{y} = 1$, and in (b), we plot the result for the second-outermost site $\tilde{y} = 1 + \frac{1}{2}$.

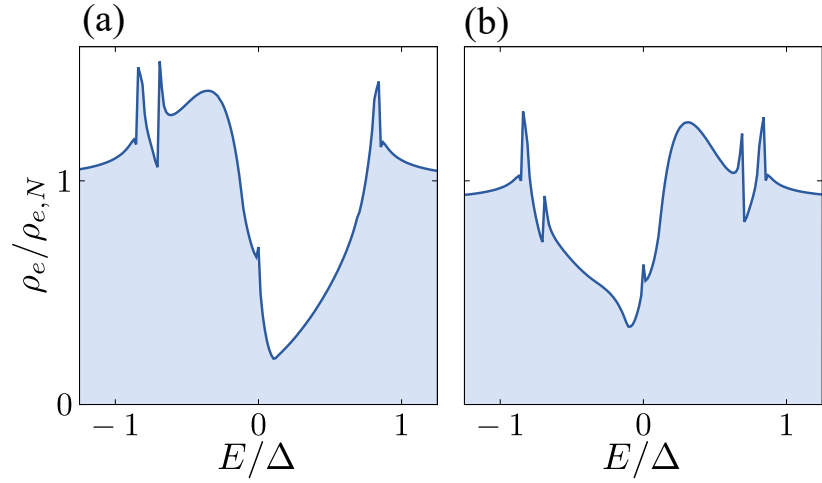


FIG. 10. Electron part of the spectral function with B_{3u} pairing symmetry as a function of the energy E . In (a), we show the result for the outermost site, i.e., $\tilde{y} = 1$, and in (b), we plot the result for the second-outermost site $\tilde{y} = 1 + \frac{1}{2}$.